Universidad Politécnica de Valencia

Escuela Técnica Superior de Ingeniería de Telecomunicaciones

Ghent University

Department of Information Technology

OPTICAL FIBER PROBE SENSORS FOR PORTABLE AND IN-VIVO DETECTION OF BIOMOLECULES

by

Cristina LERMA ARCE

Supervisors: Ir. Katrien DE VOS, Prof. Dr. Ir. Roel BAETS,
Dr. Ir. Peter BIENSTMAN,

Master thesis presented to achieve the academic degree of
TELECOMMUNICATION ENGINEER
at Universidad Politécnica de Valencia

Academic year 2008–2009

Acknowledgments

Firstly, I'd like to thank Katrien De Vos, my thesis supervisor, for the continuous help she has offered me and for the patience and comprehension she has shown me, even when I had difficulties. Many thanks also to Katarzyna Komorowska, whose explanations have given me a clear vision about how to solve each problem. She taught me a new model of work, which I'll try to use in my future research.

I would also like to express my gratitude to Prof. Roel Baets and Prof. Peter Bienstman from the Photonics Research Group in Ghent, for everything they have done to make this thesis possible and for offering me advice and support. Special thanks to Prof. Peter Bienstman, who has helped me so much, and has been a great support for me during the last difficult period.

I am also very thankful to everyone from the Photonics Research Group in Gent, for being such a helpful and cheering group and for all the useful work they've done before my arrival. Thanks also to Prof. Salvador Sales and Prof. Geert Morthier, who immediately made me feel part of the Photonics Research Group.

I'm grateful to my parents, without which efforts this experience wouldn't had been possible, and to my sister, Vicky, for encouraging and supporting me in everything I do, especially during this last year in Ghent.

Many thanks also to my friends of the UPV and in Gent, who have made my time more enjoyable. Special thanks to Irene and Almudena, who have been an unconditional support during these last years of hard work. Thanks also to Martina and Carlos, who made my erasmus year an unforgettable experience, during these last months, they have been an important part of my life and therefore also a great help in writing this thesis.

Finally, I thank Enric for giving me his strength and his joy, sharing me his ideas and his optimism that has helped me so much, and for becoming my main support during this year.

Optical fiber probe sensors for portable and in-vivo detection of biomolecules

Cristina Lerma Arce

Supervisor(s): Katrien De Vos, Roel Baets, Peter Bienstman

Abstract—**This article introduces the development of a fiber probe sensor proposed as a biosensor. The integration of a microring resonator on the tip of an optical fiber is the base of this research. A deep analysis about the requirements to fabricate this device has been performed. Simulations of the proposed sensor and its fabrication are presented.**

Keywords—**microrings resonator, grating couplers, biosensing**

I. Introduction

THE growing need for fast and cheap detection of biomolecules has been the reason why many groups have focused their investigation on the development of efficient and practical biosensors. Applications as air control, food and water control, or even monitoring biomolecular reactions in the human body, detecting viruses, toxins, bacterias.. require a practical and dynamic tool that provides a fast and reliable detection. A cheap, handy and robust sensor embodies this tool. The detection without the need of any fluidic or a complicated setup to perform the measurement and the use of this tool for in-vivo detections are also requirements of this applications. A sensor probe is proposed in this paper as the sensor able to meet all this requirements.

It consists of the adaptation of a microring resonator on the tip of an optical fiber. For that, grating couplers are needed to couple light from the fiber to the ring and viceversa. This structure is illustrated in figure 1.

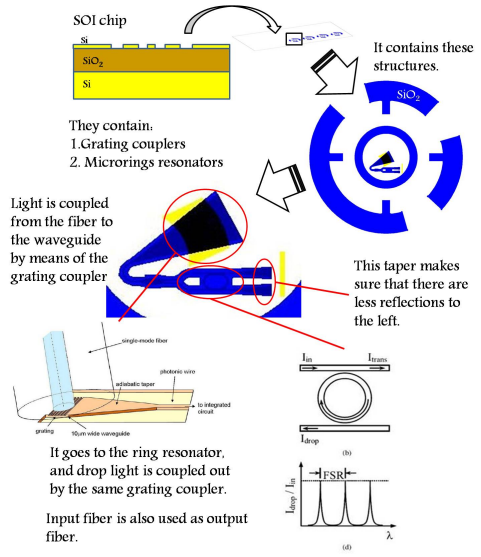

Fig. 1. Structure: Microrings resonators and grating couplers

II. Simulations

The structure of this fiber probe sensor was simulated and compared with other two sensors. One of them was a Silicon-on-Insulator chip sensor, that consists of a microring resonator on a SOI chip, and the second one was a second fiber probe sensor, where the waveguides are on top of the SU-8, rather than embedded in it. See figure 2.

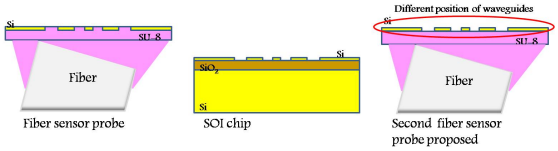

Fig. 2. Compared designs.

The literature about SOI chip sensors has demonstrated that they are the most robust labeled free sensor nowadays [1]. Indeed, results of simulations confirmed this. The sensitivity associated to SOI chip is very high. However, the SOI chip is not a practical and dynamic tool because it is needed a complicated setup to realize measurements.

The sensitivity of the second fiber probe proposed is the highest of the three structures for TE mode. The strategic position of the waveguides and the small confinement of the mode due to the small contrast of the refractive index in the structure, are two reasons that make them a bit more sensitive than SOI chip. The walls of the waveguides where the electrical field is stronger, are exposed to the changing environment, whereas in our sensor probe design, these walls are surrounded by SU-8. It explains why its sensitivity is also higher than of our sensor probe. The fabrication of this sensor would need to happen directly on the tip of the fiber, and consequently it would be more expensive.

The first fiber probe sensor is the handiest and cheapest sensor. In addition, this fiber probe could be connected to any measurement equipment in a fast and comfortable way, and carry out a fast and reliable detection of biomolecules. These are the reasons why we focused our research on them.

III. Process 1: Etching before sticking

Three different processes have been tried in order to fabricate it and to obtain good results as biosensor. Process 1: Etching before sticking, took most of the time of the work performed. It consists of four steps illustrated in figure 3.

First, a SU-8 layer is deposited over the chip, with a specific thickness. Then, a hole in this layer is made by lithography in order to create a window for the HF in the next step. Through this hole, HF will begin the underetching of the SiO_2. After this step, the fiber is aligned above the grating couplers and a glue is used to join them. This glue is cured by a UV lamp. Pulling up the fiber, we obtain our device.

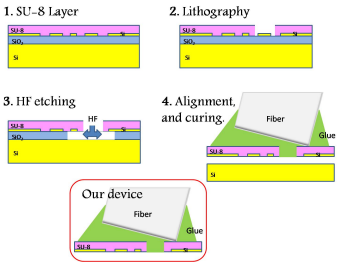

Fig. 3. General sketch process 1

The development was performed optimizing each step of the process, even another step was added, the HF dip.

Cristina Lerma is a master student at the Photonics Research Group, Department of Information Technology (INTEC), Ghent University (UGent), Ghent. The fabrication and experimental work of this research was done at Ghent University under supervision of Prof. Dr. Ir. Peter Bienstman and Ir. Katrien De Vos. This work completes the formation of the student of Telecommunication Engineering at Universidad Politécnica de Valencia. E-mail: cristtinalerma@gmail.com

An HF dip before the SU-8 layer deposition removed the possible native SiO_2 created on the Si waveguides surface. This new step optimized the adhesion of our structure to the fiber.

Measurements of the transmission after each step of the process were carried out. The signal showed resonances shifted after each step due to the change of the effective index on the sensor surface [2]. However, after HF underetching, the third step of the fabrication process, no more resonances were found. A deep investigation to find out the reason of the problem was carried out.

First idea was the replacement of the HF used, after observing that this HF could go through the SU-8 layer, underetching the sample without any lithography step. Buffered HF was proposed as solution, while another investigation about the conditions of the waveguides after the underetching was going on.

Finally, the test with buffered HF failed because it needed a long time to underetch the sample and SU-8 didn't resist. On the other hand, the results of that investigation demonstrated that the structure was collapsed after the underetching.

IV. Process 2: Etching after sticking

Process 2 was very similar to the first one. It was developed in order to avoid the collapse problem of process 1. It consists of the same five steps of the process 1, but changing the order of the two last steps. An overview of the process is illustrated in figure 4.

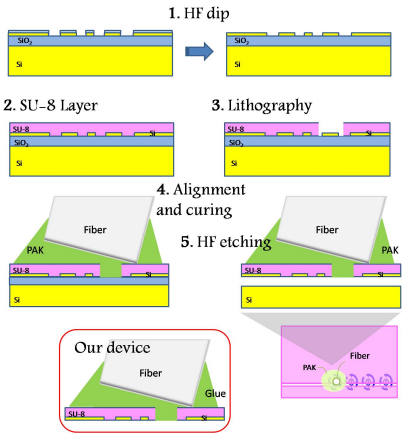

Fig. 4. General sketch process 2

Observing this sketch, the alignment and curing is before the underetching. This change regarding the first process entails the need of moving the chip and the fiber after the curing. For that reason the drop of PAK, glue used to stick fiber and chip, should be big enough to allow that the fiber held the chip. This was a problem as the big drop of PAK prevented that HF began the underetching near our structure, consequently, this step took too long time, and the adhesion between sample and fiber was damaged. SU-8 was proposed to replace PAK, but results didn't improve.

V. Process 3: Removing of Si substrate and SiO_2

Process 3, was performed as last alternative to obtain some good results. The main idea was to remove each layer of the chip from the bottom, in order to leave just the Si waveguides stuck to the fiber. This process consists of six steps that are illustrated in figure 5.

First, the thinning of the Si substrate is performed by means of grinding. Then, the alignment should be performed, but before, the previous HF dip and the SU-8 layer deposition is required. After the alignment, the sample and the fiber are introduced into a KOH solution in order to remove the rest of the Si substrate. Just Si waveguides and SiO_2 layer are left. Then the HF underetching is performed removing the SiO_2 layer.

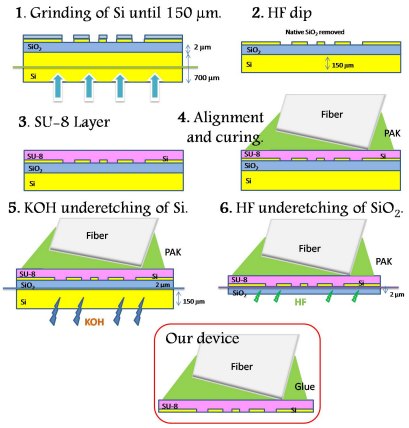

Fig. 5. General sketch process 3

Some difficulties were found developing this process. The most important was the fall of the sample after some time in KOH. The immersion into KOH should be approximately 150 min to remove the 150 μm of Si substrate left after the grinding. PAK, used as glue, came unstuck after one hour into KOH. The replacement of PAK by SU-8 didn't improve the results, but it resisted a bit more.

The proposition of using the ICP, to thin the Si substrate to 50 μm, and thus, to make shorter time required in KOH didn't work. Waveguides were damaged in the process, and they couldn't be protected.

The need of protection of the sample and the fiber from KOH was the only possible solution. For this, wax was used to cover the sample and the fiber. The next problem found was the melting of the wax at 75^{o}C, temperature of KOH solution required to underetch Si. The wax melted went underneath the sample making impossible the underetching. After 150 min of immersion, the sample wasn't underetched at all.

VI. Conclusions and perspectives

Despite the lack of success at this stage, many processes were developed, and three promising future lines of research have been identified:

1. The research on the optimization of the SU-8 layer thickness that avoids the collapse of our structure.

2. Possible redesign of the mask used during the lithography. A possible option is illustrated in figure 6. The first aperture done near the rings could control the size of the drop, allowing the HF underetching by means of the second aperture. A redesign of the chip would be also necessary, to add SiO_2 where the apertures would be done.

Fig. 6. Possible design for a future mask

3. The research on a product that resists KOH, and protects SU-8, sample and fiber would solve our problem, providing as result our device.

The work performed in this thesis provides an excellent basis from which to start this research.

VII. Acknowledgments

The author would like to thank Prof. Dr. Ir. Peter Bienstman, Ir. Katrien De Vos and Dr. Katarzyna Komorowska for the constant help received.

References

[1] K. De Vos, I. Bartolozzi, E. Schacht, P. Bienstman, and R. Baets., "Silicon-on-insulator microring resonator for sensitive and label-free biosensing.," *Optics Express*.

[2] F. Vollmer, D. Braun, and A. Libchaber., "Protein detection by optical shift of a resonant microcavity.," *Applied Physics Letters*, vol. 80(21):40574060, 2002.

Contents

Chapter 1

Background

1.1 Introduction

Nowadays there exists an increasing need for efficient sensors, specifically for biomolecular detection. During the last decades these sensors have been developed and improved at laboratories, but today they should be adapted to the actual and real needs. Many applications require cheap, robust and handy sensors that offer a high sensitivity with an immediate and easy measurement. Some of this applications can be air, water or food control, or even monitoring biomolecular reactions in the human body, detecting viruses, toxins, bacteria.. The objective of this thesis will be the development of a fiber sensor, sensor which will be able to meet all this requirements previously cited. This fiber probe will consist of a sensor on the tip of an optical fiber that, consequently, will be handy, flexible, easily transportable, easily connectable to optical equipment and it will provide a cheap and fast detection. To accomplish this objective a complete study about actual optical biosensors is required, which is described in the following paragraphs.

1.2 Optical Biosensors

Biosensors are a interesting field where many groups have focused their attention on. Sensing techniques based on labelled detection are well known for their high resolution and easy detection of biomolecules [1]. This sensing technique depends on labelling the analyte molecules with fluorescent or radio-active materials. The analyte molecules can then easily be detected using luminescence techniques that offers the best resolutions for sensing of

biomolecules such as proteins. However, sensing methods based on luminescence have some drawbacks which make them unattractive for robust, fast and cheap sensors. A first drawback is that the extra labelling step increases complexity and reduces reliability of the sensing method. Secondly, antibodies used for labelling can be very expensive, which is an important disadvantage. This is one of the principle reasons why label-free sensors are more interesting.

Label-free detection is based on the fact that the refractive index of biomolecules is higher than of water. On binding of molecules, the refractive index adjacent to the sensor surface, is increased and it can be detected in real time. Label-free detection techniques are powerful tools to monitoring and quantifying surface mass deposition in real time with detection limits of a few pg/nm^2. [2]

The most important label-free sensors are based on surface plasmon resonance (SPR), interferometry and resonant microcavities. In this chapter, we will emphasis on biosensors based on microcavities in order to describe in detail what has been used to develop this thesis.

1.2.1 Biosensors based on microcavities

Recently, several groups have proposed sensors based on resonant microcavities. The sensing effect is enhanced compared to waveguide sensing or SPR because of the multiple passing of light through the sensing section. This allows reduction in size by several orders of magnitude, which greatly reduces the amount of analyte needed for detection.

Vollmer [3] has demonstrated protein detection with a resonant silica microparticle of spheroidal shape (diameter $\sim 300\mu m$). The whispering gallery modes in the microparticle were excited by evanescent coupling to an optical fiber. The resonances of the microparticle were found to have a quality factor of $Q \sim 2 \times 10^6$. A shift of the resonances towards longer wavelengths occurs when adsorption of biomolecules on the particle's surface causes its effective circumference to increase. The operation as a biosensor was demonstrated with the use of streptavidin as a target analyte and biotinylated bovine serum albumin (BSA-biotin) as a recognition element [1]. The ability to respond to a monolayer of biomolecules is shown on the basis of an initial wavelength shift

[1] the avidin/biotin or streptavidin/biotin system is often used for surface sensing experiments, because of its extremely high affinity constant ($K_a \sim 10^{15} M^{-1}$) and the possibility to couple biotin to a variety of proteins without changing their biological activity.

after adsorption of BSA-biotin and a second shift after injection of a streptavidin solution to the sample.

Microrings as biosensors

The large quality factors of microspheres make them potential candidates for high sensitivity sensing. However, microspheres are not suited for integration and only a part of the adsorbed molecules have an effect on the waveguide modes resonance shift [3]

As an alternative, microrings has been proposed. Although they have lower quality factors, they have excellent integration capability and are easier to fabricate.

Next section will introduce some characteristics and requirements of these microrings resonators, and will describe them in detail.

1.3 SOI in integrated photonic circuits

According to the last section, resonant microcavities are one of the most sensitive and efficient techniques for free label biosensing. Microrings resonators are able to detect very small concentrations of biomolecules in the tested environment. This section describes which characteristics are required to make them the efficient biosensors that we have used to develop this thesis.

SOI chips, microrings resonators and grating couplers will be explained in detail in order to understand perfectly the structure of our final device, optical fiber probe sensor, and how it works.

1.3.1 SOI

Silicon-on-Insulator (SOI) is a very interesting material system for highly integrated photonic circuits. The high refractive index contrast allows photonic waveguides and waveguide components which guide, bend and control light on a very small scale so that various functions can be integrated on a chip. Moreover SOI offers a flexible platform for integration with surface plasmon based components which in turn allows for even higher levels of miniaturization. The mode distribution of the guided modes is such that a substantial portion of the light is concentrated outside the core material, making them suitable for sensitive detection of environmental changes. This allows a high

level of miniaturization, which is advantageous. For example, the sensitivity of e.g. a PIC based strain sensor increases with decreasing radius of ring resonators on the PIC. Light can be efficiently coupled in and out the PIC by use of e.g. a grating coupler (see further) or another coupling element.

Using Silicon-on-Insulator also has some technological advantages. Due to the CMOS industry, silicon technology has reached a level of maturity that outperforms any other plane chip manufacturing technique by several orders of magnitude in terms of performance, reproducibility and throughput. Nanophotonic integrated circuits can be fabricated with wafer scale-processes, which means that a wafer can contain a high number of photonic integrated circuits. Combined with the commercial availability of large wafers at a relative moderate cost, this means that the price per photonic integrated circuit can be very low. This is a significant economic advantage when producing integrated photonic circuits to be used as part of the optical sensor probe .

1.3.2 Microrings Resonator

Introduction

The mechanism of light propagation in a microring is comparable to that in an ordinary dielectric waveguide. A waveguide basically consists of a core where the light is confined, surrounded by materials of lower refractive index. From Maxwell's theory, it is known that there exists a discrete number of so-called waveguide modes. These are field shapes whose field distribution and polarization do not change while propagating through the waveguide. The field of these modes is confined to the high-index core region and decays exponentially into the surrounding materials. This exponential tail is called the *evanescent field* of the waveguide mode, and it is this evanescent field that is used for sensing biomolecules (see further). Each mode has its own propagation constant $\beta = k_0 n_{eff}$, where n_{eff} is the effective refractive index of the mode. For a guided mode, n_{eff} always fulfills the condition $n_{core} > n_{eff} > n_{clad}$, where n_{clad} is the highest refractive index of the materials surrounding the core. For a one-dimensional structure (a slab waveguide), Maxwell's equations become uncoupled and give rise to two classes of modes: TE modes with the electric field vectors in transverse direction and TM modes with the magnetic field vectors in transverse direction. In a waveguide with confinement

in both transverse directions, there exist still modes with a predominant TE or TM character. These are called TE- or TM-like modes.

Microrings

A ring resonator essentially consists of a looped waveguide. Just like in a straight waveguide, the light is confined to the core and decays exponentially in the surrounding material. When the phase shift after one roundtrip in the ring is an integer multiple of 2π, the light will build up in intensity due to constructive interference and will form a resonant mode of the resonator. The resonance condition becomes

$$\lambda_{res} = \frac{2\pi R n_{eff}}{m} = \frac{L n_{eff}}{m} \qquad m \in \mathbb{Z} \tag{1.1}$$

where R is the outer radius of the ring and L is its circumference.

Microcavities are usually coupled to an input or excitation waveguide which excites the field in the resonator by the evanescent tail of the waveguide mode. Sometimes, the resonator is also coupled to an output or drop waveguide. The transmission spectrum of the input waveguide will show dips at the resonance frequencies of the microcavities, since at these frequencies energy is extracted from the waveguide to the ring. In the spectrum of the drop waveguide on the other hand, there will be peaks at these resonant frequencies.

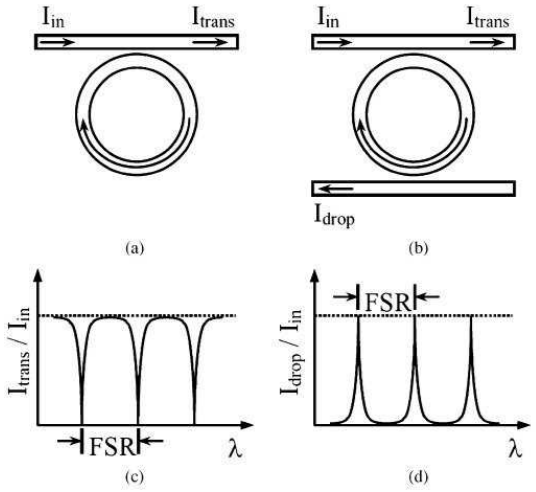

Figure 1.1: The two basic configurations of a microring resonator and its transmission spectra: (a) singly coupled microring, (b) doubly coupled microring, (c) spectrum at the transmission port, (d) spectrum at the drop port, [4]

The configurations with and without drop port and the corresponding spectra are shown in figure 1.1.

The spectral distance between two modes with a subsequent mode number m is called the free spectral range (FSR) and is given by the equation

$$FSR = \frac{\lambda^2}{2\pi R n_{eff}} \tag{1.2}$$

The width of the resonance peaks is described by their quality factor Q, defined as the ratio of the energy stored in the resonator to the energy loss per cycle. The Q factor can be calculated with the formula

$$Q = \frac{\lambda_{res}}{\delta\lambda_{FWHM}} \tag{1.3}$$

where $\delta\lambda_{FWHM}$ is the width of the peak (dip) at half of its maximum (minimum) value (FWHM = Full Width at Half Maximum/Minimum). A high Q factor thus corresponds to narrow spectral peaks.

The width of the resonance peaks can also be described by the finesse F of the resonator, defined as

$$F = \frac{FSR}{\delta\lambda_{FWHM}} \tag{1.4}$$

In figure 1.2 these parameters are illustrated.

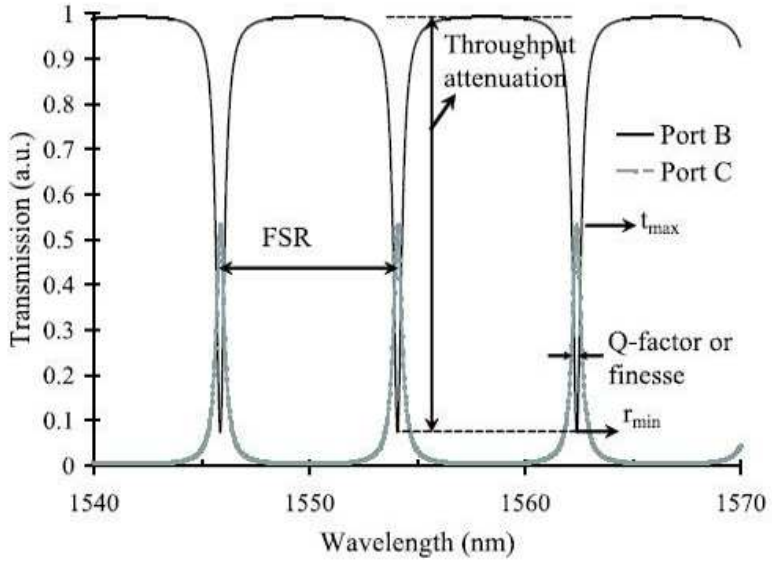

Figure 1.2: Parameters of the signal received.[5]

From the resonance condition 2.1, we can derive that

$$\delta neff/neff = \delta\lambda_c/\lambda_c \sim 1/Q \qquad \delta\lambda_c \neq \delta\lambda_{FWHM} \qquad [4] \tag{1.5}$$

The detectable refractive index changes are thus inversely proportional to the quality factor of the cavity. Consequently, for a resonator to be used as a sensor, high Q factors are important to minimize the minimal detectable wavelength shift and therefore the sensors sensitivity. Thus they also will be less sensitive to noise. To achieve high Q factors, all the resonator losses have to be minimized. Typical occuring losses in ring resonators are bending and surface losses. Surface losses are due to surface roughness and can be alleviated with better fabrication techniques. Bending losses will increase with smaller radii (since the mode is pushed outwards), while surface losses will be reduced due to the smaller roundtrip lenghts. Generally, it is assumed that Q factors of minimum 1500 are needed to make a useful biosensor. [6]

Concerning the dimensions of a resonator, it can be related with their sensitivity as biosensor. This relation has been assessed by De Vos [7]

A distinction is made between sensitivity for bulk refractive index changes (homogeneous sensing) and sensitivity for a layer of adsorbed molecules (surface sensing) of mass $M = \rho Sh$, where ρ is the mass density of the molecular layer, S is the sensing area and h is the layer thickness. From the resonance condition of a ring resonator 2.1 it follows that

$$\Delta n_{min} = \frac{m}{L}\left(\frac{\partial n_{eff}}{\partial n_{bulk}}\right)^{-1}\Delta\lambda_{min} \tag{1.6}$$

$$\Delta M_{min} = \rho S\frac{m}{L}\left(\frac{\partial n_{eff}}{\partial h}\right)^{-1}\Delta\lambda_{min} \tag{1.7}$$

The factor m/L in the above expressions is a constant, since the cavity mode orde m is assumed to scale linearly with the circumference L. The minimal change in bulk refractive index $\Delta\lambda_{\min}$ is independent of the microrings dimensions. The minimal detectable absorbed mass $\Delta M_{\min}$ does however scale with the area S. This implies that with a smaller resonator, smaller concentrations can be measured.

1.3.3 Grating couplers

Grating couplers are optical components which are gaining more and more importance in telecommunication as well as in sensor technology. They have been proposed as a solution for the problem of coupling light between optical fibers and waveguides. The large difference in dimensions between the fiber and the waveguides on a chip causes high insertion losses and costs and the ongoing trend to make components smaller, in order to integrate them on one single chip, makes the problem even more difficult.[8] We use grating couplers for out-of-plane coupling between a standard single-mode fiber and a SOI waveguide. The coupling principle is shown in figure 1.3. This grating couplers

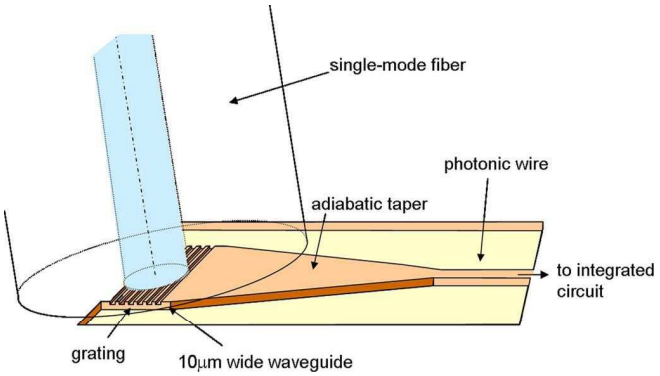

Figure 1.3: Coupling principle between fiber and photonic wires by means of a grating.[8]

are designed for light with TE polarization and give a maximum coupling for an input angle of 10 degrees. At this angle, the central wavelength of the coupling curve is around 1550 nm, with a 1dB bandwidth of approximately 40 nm. The central wavelength shifts towards longer wavelengths if the angle is decreased. The maximal fiber-to-waveguide transmission is about 30%. For a fiber-to-fiber transmission, this yields an overall efficiency of about 9% [9] The grating is etched on a wide waveguide which guides the light with an adiabatic taper into the excitation waveguide. This waveguide consists of a 220-nm-thick silicon core on top of a buried oxide layer on a silicon substrate (SOI).

1.4 Optical fiber probe sensor

It was mentioned in the introduction that the objective of this thesis is the development of a cheap, robust and handy sensor with a high detection sensitivity. It consists of the adaptation of a SOI microring resonator on the tip of an optical fiber. It will be well understood after looking the following sketch.

1. SOI chip that contains microrings resonators.

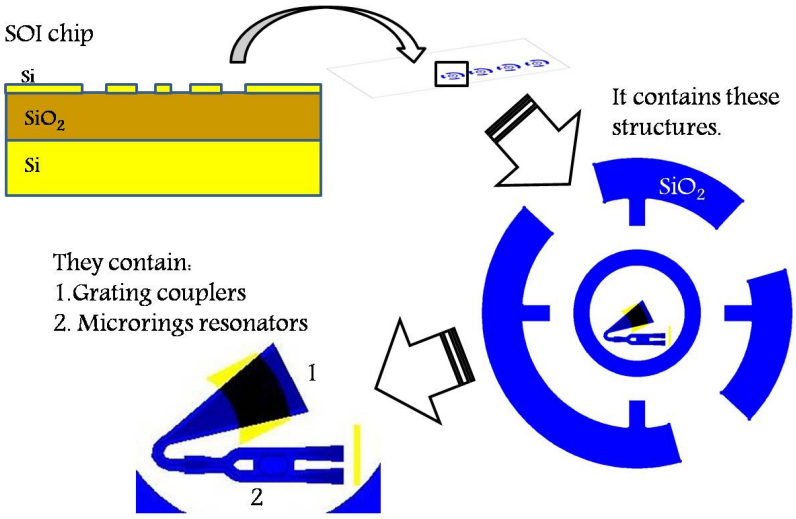

Figure 1.4: SOI chip that contains microring resonators.

2. How light travels.

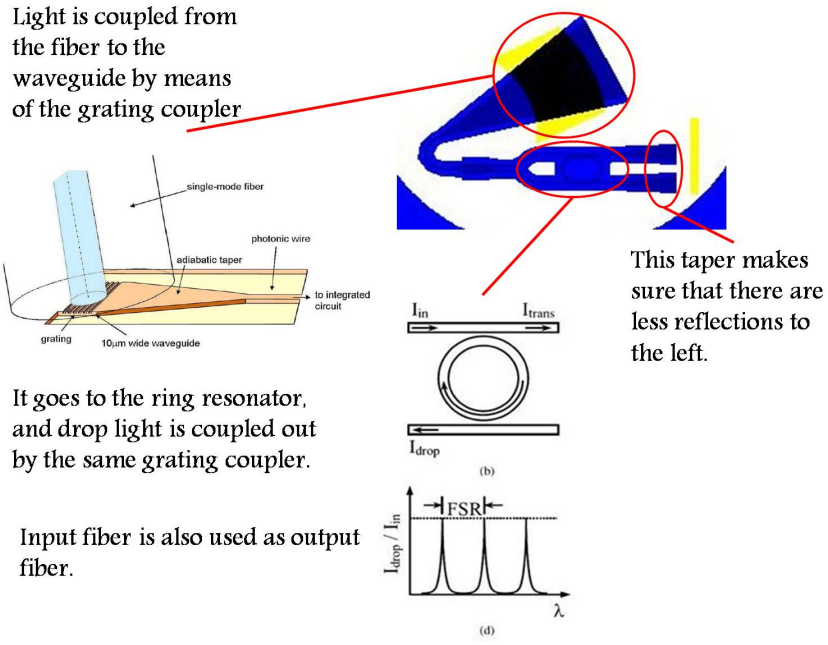

Figure 1.5: How light travels.

3. After many processes which will be explained in chapter 3 Fabrication and measurements, silicon waveguides from the SOI chip are transported to the tip of an optical fiber. The following picture illustrates it.

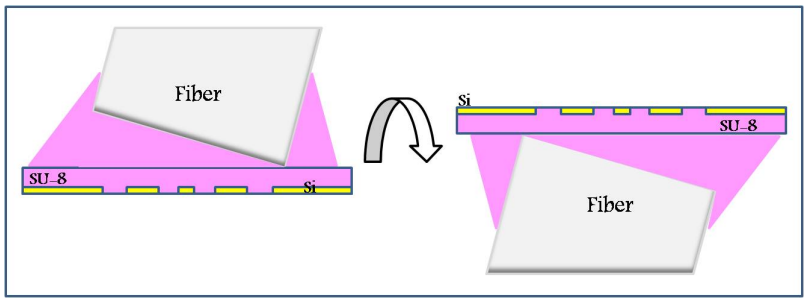

Figure 1.6: Fiber probe sensor.

This is the device proposed. It will be tested and compared with other two competitive models whose stuctures are described in figure 1.7 and figure 1.8.

SOI chip sensor: This sensor consists of a microring resonator on a SOI chip.

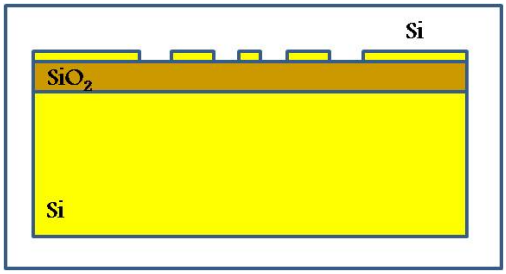

Figure 1.7: SOI chip sensor.

Second fiber probe sensor: This is a device very similar to the previously proposed, but there is a small difference in the position of the silicon waveguides.

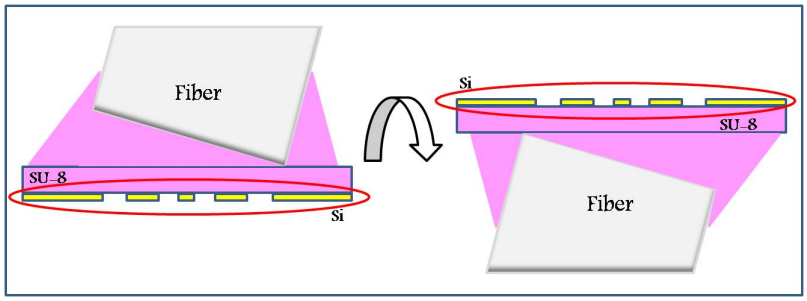

Figure 1.8: Second fiber probe sensor proposed.

During the development of the thesis, simulations and comparisons of these models, the fabrication and measurements carried out to test our device will be explained in detail. Then, this thesis will be completed with the corresponding conclusions.

Chapter 2

Simulations

2.1 Introduction

This chapter describes the method used to simulate the performance of the sensor probe developed in this thesis. We compare characteristics of three different models of label free sensors, and elucidate their most significant advantages and drawbacks.

Firstly, it's necessary to describe two sensing mechanisms that are distinguished: homogeneous sensing and surface sensing.

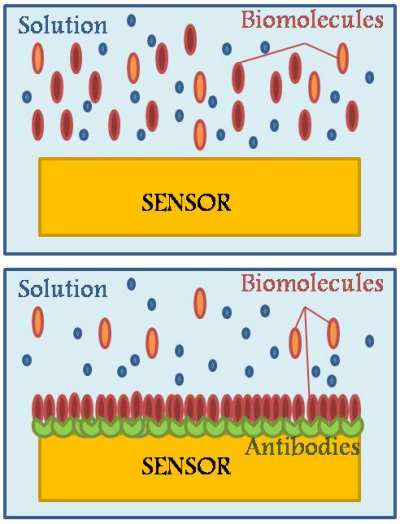

Figure 2.1: Bulk and surface sensing, respectively.

In homogeneous or bulk sensing, the sensor surface is homogeneously covered with an analyte solution. This will change the bulk refractive index of the top medium and this will affect the effective index of the guided mode. A drawback of this method is that all materials in the solution will contribute to the wavelength shift, which implies that the sensor is not specific to any particular target molecule. In surface sensing, this problem is solved by attaching recognition molecules, called receptors or antibodies, to the sensor surface. These receptors can selectively bind specific biomolecules. Unbound molecules can be rinsed off, so that only the biomolecules bound to the sensor surface contribute to the effective index change. Ac-

cordingly, surface sensing enables specific and label-free detection. Figure 2.1 illustrates these differences between bulk and surface sensing.

In this chapter, both sensing mechanisms have been considered using the three different biosensor models described at the introduction of this thesis.

2.1.1 FimmWave

Firstly, is important to mention the programm used to develop this part of the thesis, it is called FimmWave. FimmWave is an electromagnetic simulation tool based on Eigenmode Expansion and Propagation. It is a fully vectorial mode finder for 2D waveguide structures, which may be of almost any geometry or material, such as SOI, polymer and etched GaAs/AlGaAs waveguides, as well as single and multicore fibres. It allows the tackling of problems with strong variations in refractive index, thin layers, etc. with comparatively small computational effort.

2.2 Models

As mentioned in the introduction of this chapter, three different biosensor models have been simulated using FimmWave. All of them are analyzed and compared, we will discuss their sensitivities and capabilities for their use in real life.

According to the previous chapter, the detection of biomolecules is measured by resonance wavelength shifts. The effective index changes when biosensors are introduced to another environment where biomolecules are present, producing these mentioned wavelength shifts. The formula that define these shifts is shown bellow. [10]

From resonance condition:

$$\lambda_{res} = \frac{2\pi R n_{eff}}{m} = \frac{L n_{eff}}{m} \qquad m \in \mathbb{Z} \tag{2.1}$$

follows

$$\Delta\lambda_{res} = \frac{\Delta n_{eff} L}{m} \tag{2.2}$$

Due to dispersion, this wavelength change also has an effect in n_{eff}. In a first order approximation we can decouple both effects, and considering that the variation of n_{eff} is also dependent on n_g. It's possible to write:

$$\Delta\lambda_{res} = \frac{\Delta_{env} n_{eff} \cdot \lambda_{res}}{n_g} \tag{2.3}$$

Thereby, simulations are needed to quantify these shifts. The simulation method is the following: The cross-section of the structure of each model is employed to simulate electromagnetic modes in the waveguides. The fundamental mode, TE, is used to find out the effective refraction index of the mode and the group index of it in order to obtain the wavelength shift following equation 2.3.

We also have considered TM modes, although the grating couplers used just provides high coupling efficiency for TE modes (see subsection 1.3.3).

These are the three structures we compared.

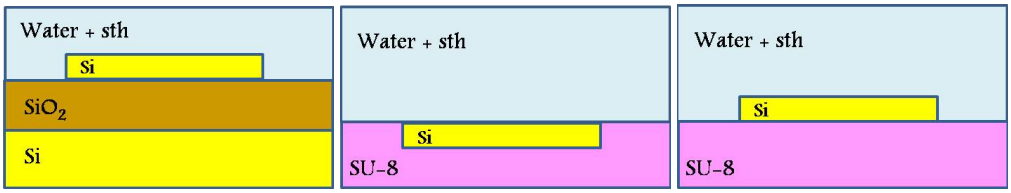

((a)) SOI chip ((b)) Fiber probe ((c)) Second fiber probe proposed

Figure 2.2: Bulk sensing

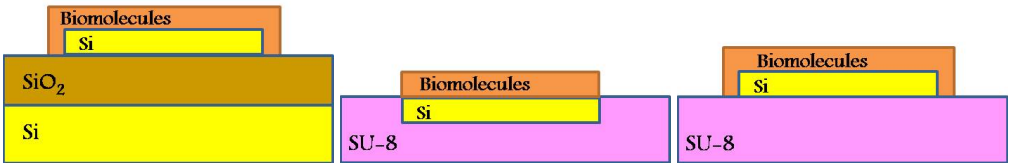

((a)) SOI chip ((b)) Fiber probe ((c)) Second fiber probe proposed

Figure 2.3: Surface sensing

The information about thickness and effective refraction index considered for each layer are presented in the (see table 2.4).

	n_{eff}	Thickness (um)
Water	1,311	2
Biomolecules	1,4	0-0,04
Si	3,47	0,22
SU8	1,57	0,44
SiO_2	1,44	2

Figure 2.4: Details of each layer

2.2.1 SOI chip sensor

Figures 2.2(a) and 2.3(a) are the structures used to simulate the model SOI chip sensor for bulk sensing and surface sensing respectively.

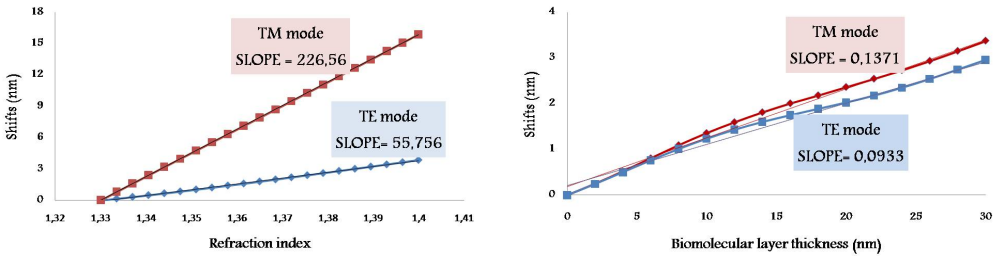

((a)) Bulk: Changes at the environment.

((b)) Surface: Changes of biomolecular layer thickness.

Figure 2.5: SOI chip sensor

The slopes of the functions (see graphs 2.5) provide us information about the shift of the resonance wavelength when a unit of refraction index for bulk sensing, or a nanometer of the biomolecules layer thickness for surface sensing, has changed. Therefore, a more robust sensor will have a greater number, which means, it will be able to detect a smaller variation in the environment, in other words, it will have a better sensitivity.

In this case, slopes of the functions tell us that SOI chip sensors have a good sensitivity, but they will be compared with the rest of the structures.

2.2.2 Fiber Probe

This is the model of the device developed in this thesis. Its structure is illustrated in figure 2.2(b) for bulk sensing, and in figure figure 2.3(b) for surface sensing.

Concerning the sensitivity of the fiber sensor probe, it is easy to see a big drop in the detection limit with respect to the latter model (see graphs 2.6 and compare with graphs 2.5)

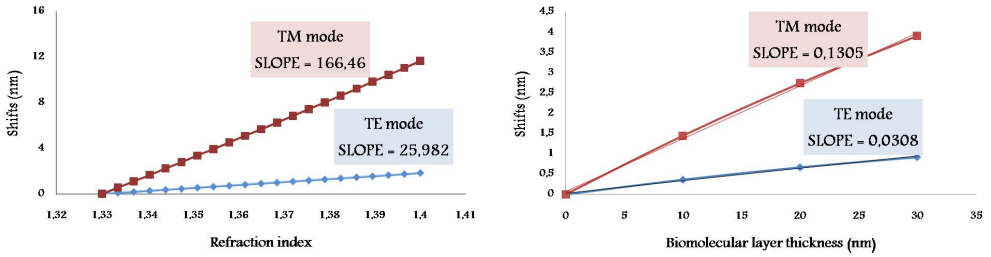

((a)) Bulk: Changes at the environment.

((b)) Surface: Changes of biomolecular layer thickness.

Figure 2.6: Sensor Probe

This fact was expected, due to the great differences between the structures. Here, silicon waveguides are on SU-8 instead of SiO_2 in SOI chip sensor. This means an increase in the effective refractive index of materials, and also in the group refraction index. According to the equation 2.3, this provokes a different wavelength shift. Despite this drop, this structure presents other advantages that first structure doesn't have. This sensor is able to detect biomolecules in a fast, easy and reliable way, and moreover, it is handy, flexible and cheap. In the last section 2.3, it will be compared to the rest of the structures.

As the sense of this structure is rather low, we propose a different structure, which we will analyze now.

2.2.3 Second fiber probe proposed

Figures 2.2(c) and 2.3(c) show the structures employed to carry out the simulations for this model, for both methods of sensing.

With regard to the results of simulations for this model, indeed, the sensor sensitivity has improved. This improvement was expected and it was the reason of the proposal of this second fiber probe.

Looking at figures 2.2(c) and 2.3(c) the silicon structure is above SU-8 layer. Vertical walls of the silicon structure are exposed to the changes in the environment, whereas in our sensor probe (look 2.2(b) and 2.3(b)) these walls are surrounded by SU-8. This exposition to the changes in the environment makes these sensors more sensitive, because the electrical field is stronger in these vertical walls. Besides the mode is less confined due to the small contrast in the refraction index.

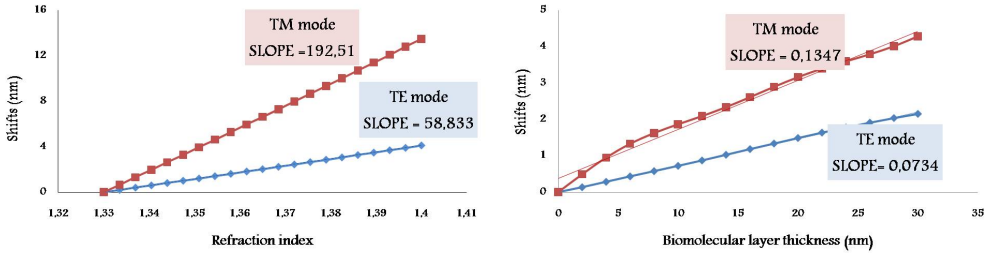

((a)) Bulk: Changes at the environment.

((b)) Surface: Changes of biomolecular layer thickness.

Figure 2.7: Second sensor probe proposed

Instead, the fabrication process to obtain this fiber sensor is quite more difficult than the last one, and, in addition, more expensive. The fact of the Si layer is above SU-8, unlike our sensor probe, makes them to require a greater complexity in its fabrication.

2.3 Comparing structures

This subsection compares the simulation results of each structure described above. For that, the tables below show the numbers of the slope of each graph, which, as before has been explained, gives us information about the sensitivity of each sensor.

TE mode	Bulk sensing	Surface sensing
SOI chip	55,756	0,0933
Fiber Probe	25,982	0,0308
Fiber Probe 2	58,833	0,0734

Figure 2.8: Comparisons. TE mode

TM mode	Bulk sensing	Surface sensing
SOI chip	226,56	0,1371
Fiber Probe	166,46	0,1305
Fiber Probe 2	192,51	0,1347

Figure 2.9: Comparisons. TM mode

The literature about Silicon-on-Insulator chip sensor has demonstrated that they are the most robust labeled free sensor nowadays. Indeed, observing the

results of simulations (see graphs 2.5), its sensitivity is very high. Nonetheless and despite this properties, it is not possible to make of them a practical and dynamic tool because it is needed a complicated setup to realize measurements.

The handiest and cheapest structure, is the sensor probe proposed in this thesis. This sensor probe is possible to be connected to any measurement equipment in a fast and comfortable way , and carry out a fast and reliable detection of biomolecules, even in an in-vivo process. However its sensitivity is approximately 2 times worse than of the SOI structures.

On the other hand, the sensitivity of the second fiber probe sensor proposed, is even a bit higher than the SOI chip for TE mode. The strategic position of the waveguides and the small confinement of the mode due to the small contrast in the refraction index are two reasons that make them very sensitive. However, it's fabrication is more complex and expensive. We will not consider it in our experiments.

Concluding this chapter, the fiber sensor probe proposed in this thesis will provide what it is expected: a handy, cheap, easily connectable and transportable sensor that will be able to detect biomolecules in a changing environment.

Chapter 3

Fabrication and measurements

This chapter consists of an introduction to the fabrication methods developed for this thesis and a detailed description of the setup used to carry out the required measurements.

This work has been performed in the Clean Room of the Photonics Research Group in Ghent University. A clean room is an environment, typically

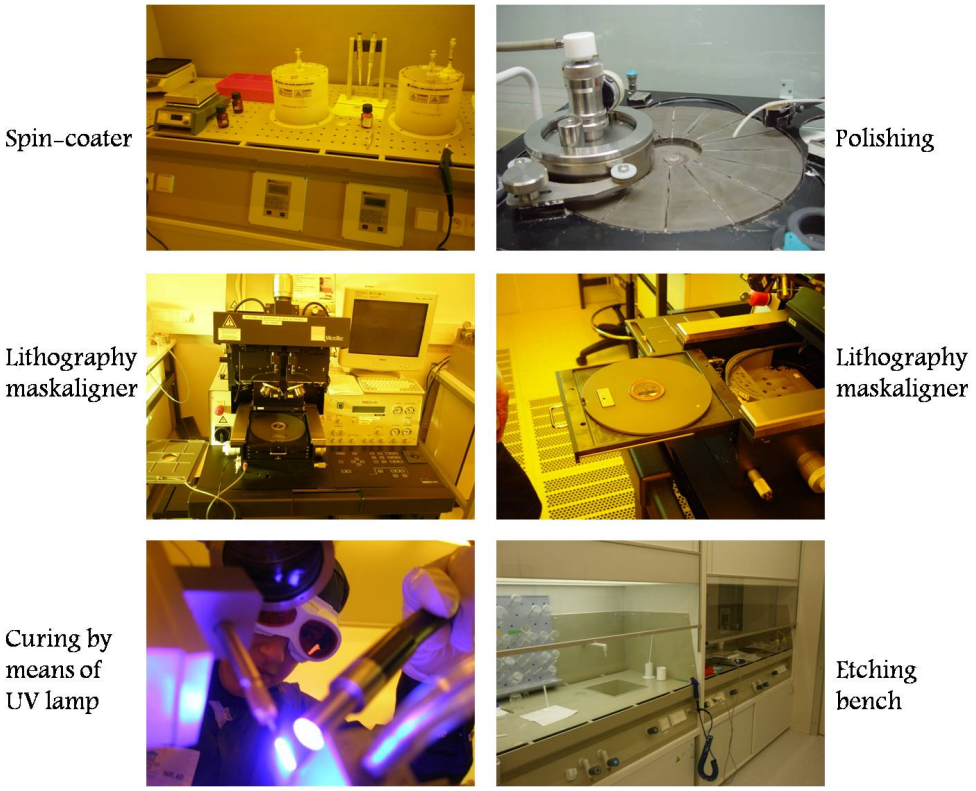

Figure 3.1: Clean room [5]

used in manufacturing or scientific research, that has a low level of environmental pollutants such as dust. The equipment of this clean room includes a high resolution photolithography maskaligner, plasma etching and reactive ion etching system, wafer thinning and polishing, among others.

The fabrication of our device required a lot of processes over the chip using this equipment. Some pictures show these processes in clean room in figure 3.1.

The fabrication of our device has been the hardest part of this thesis. Three different processes have been developed in order to obtain the final device.

One of the specific treatments over the chip was the lithography. This process is performed by the maskaligner and consists of the exposure of some parts of a chip to specific wavelength of UV light. A specific mask located between sample and light source determines which parts of the chip are exposed or not, printing a pattern over the chip. SU-8 was a product deposited on the chip before this lithography. A deep study about its treatment was required before begin fabrication. Also the underetching of some layer of the sample by means of HF or other products, has been a basic step in our processes.

Processing, problems, solutions and conclusions will be explained in detail in the following three chapters corresponding to each process. They are:

1. Chapter 4: Process 1: Etching before sticking.
2. Chapter 5: Process 2: Etching after sticking.
3. Chapter 6: Process 3: Removing of Si substrate and SiO_2.

Before these chapters, it is necessary to explain how the measurements has been performed, in certain moments of each process. Next section, will describe the measurement setup and will illustrate the procedure to obtain measurements.

3.1 Measurements

3.1.1 Measurements setup

An overview of the measurement setup used for this part of the thesis is shown in figure 3.2. A tunable external cavity laser serves as a light source to the system. A single-mode (SM) fiber guides the laser output via a polarization controller and a circulator to the input of the sample stage. The laser light is coupled from the fiber into the excitation waveguide by means of a grating

coupler (see 1.3.3). The input fiber is also used as output fiber, thus light is coupled out by the same grating coupler to the same fiber going to the circulator, that allows the light to arrive at a Newport dual-channel 2832-C power meter. It's connected by a GPIB interface to a PC where LabView is the measurement and control software.

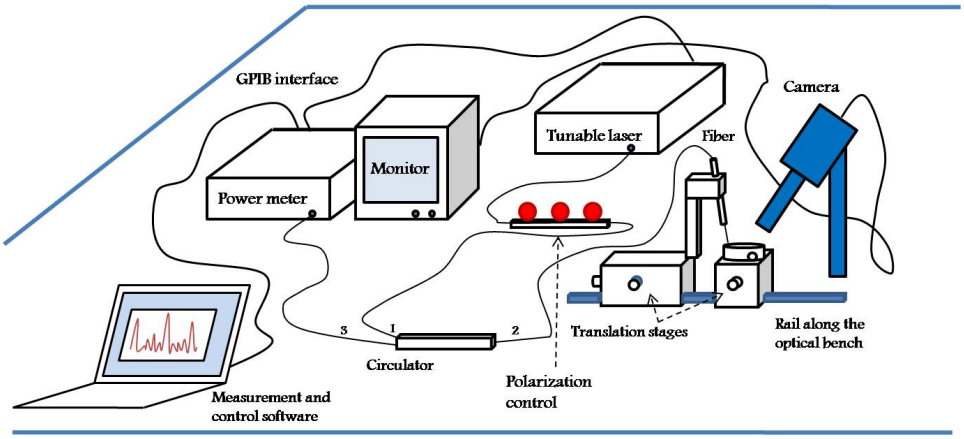

Figure 3.2: Measurement setup

The sample is fixed on a chuck that allows one to vary the horizontal angle to optimize the alignment. The sample stage itself is placed on a XYZ stage. The fiber is held by a fiber chuck at an angle of 10^o with the axis normal to the sample. This fiber chuck is also mounted on XYZ translation stage.

A camera is used in order to visualize structures and the fiber. A lamp illuminates the sample and the fiber with somewhat diffuse light. The image from the camera is displayed on a monitor.

3.1.2 Measuring spectrum

To measure the spectrum, a tunable laser is used to scan the desired wavelength range step by step. For each wavelength, the output power is recorded with the power meter. The tunable laser is automatically operated by LabView program that allows to adjust the wavelength range and the step size. An alternative is to use a broadband SLED as a light source and to measure the spectrum with a spectrum analyzer. The latter method is faster and provides a better signal-to-noise ratio. Nonetheless, the possible maximum resolution with the spectrum analyzer is only 60 pm, whereas the tunable laser has a resolution of 1 pm.

The measurement of the spectrum will be an important tool when developing the process to fabricate our device. Therefore, we describe it in detail.

The aim is to determinate where and with which power resonances were detected measuring an original sample. The setup described above was used, but the light source of the system was a SLED configured at 1550 μm, the wavelength for which microrings are designed. A power meter was used until one maximum of the signal was found, and then it was replaced by a spectrum analyzer to show the shape of the spectrum at this moment.

The best results obtained at that moment can be observed in the following graph.

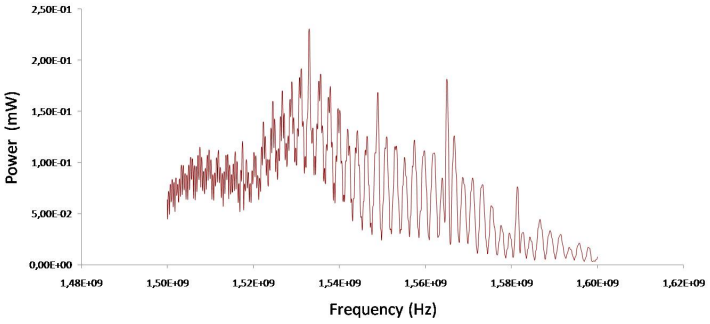

Figure 3.3: First resonance wavelength detections

In this graph, it is possible to distinguish clearly the detected resonances. It was a good beginning to determinate the optimal angle that increases the signal-to-noise ratio (SNR) of the detected signal. This was chosen at 30^o.

Once known that the procedure of the detection was correct, the setup was again the one described in section 3.1.1, where the light source was a tunable laser.

Chapter 4

Process 1: Etching before sticking.

This process was the first idea that took most of the time of the work performed.

In section 4.1, Sketch, an overview of this process will be illustrated.

In section 4.2, Process, each step will be deeply studied.

In section 4.3, Development, results, improvements and problems will be explained.

4.1 Sketch

As it has been mentioned in section 1.4, Optical fiber probe sensor, our device consists of an optical fiber where on its tip, a microring resonator and grating coupler will be integrated, in order to obtain a handy, cheap and robust sensor.

Figure 4.1 illustrates a general sketch of the process. It consists of four steps. First, a SU-8 layer is deposited over the chip, with a specific thickness. Then, a hole in this layer is made by lithography in order to create a door for the HF in next step. Through this hole, HF will begin the underetching of the SiO_2. After this step, the fiber is aligned above the grating couplers and a glue is used to join them. This glue is cured by a UV lamp. Pulling up the fiber, we obtain our device.

After observing this sketch, the name of this process 'Etching before sticking' is more understandable. This four process were independently studied in or-

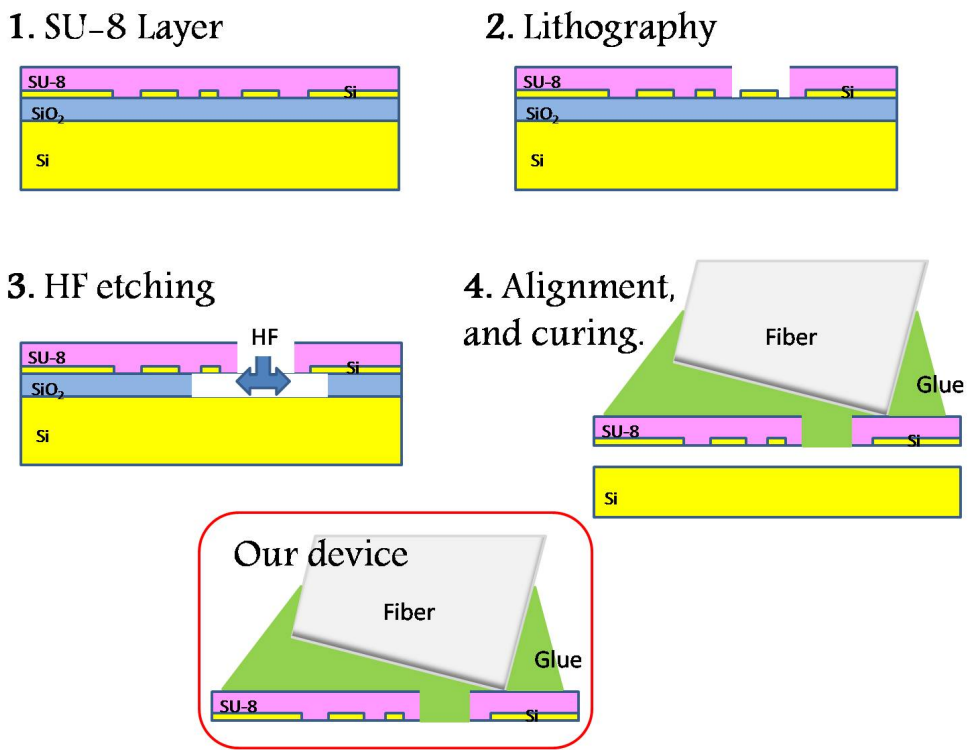

Figure 4.1: General sketch process 1.

der to be able to optimize the process in a easier way in view of difficulties. At following section each step will be explain in detail.

4.2 Process

4.2.1 SU-8 layer deposition

SU-8 is a commonly used epoxy-based negative photoresist. It is a very viscous polymer that can be spun or spread over a thickness ranging from 1 micrometer up to 2 millimeters and still be processed with standard contact lithography.

It is normally processed with conventional near UV (350-400nm) radiation, although it may be imaged with e-beam or x-ray. i-line (365nm) is recommended. Upon exposure, cross-linking proceeds in-two-steps (1) formation of a strong acid during the exposure process, followed by (2) acid-initiated, thermally driven epoxy cross-linking during the post exposure bake (PEB) step. SU-8 is highly transparent in the ultraviolet region allowing fabrication of relatively thick (hundreds of micrometers) structures. [11]

A normal process is:

1. Spin coat.
2. Soft bake.
3. Exposure.
4. Post expose bake (PEB).
5. Development.
6. Hard bake.

The last step, hard bake, is recommended to further cross-link the imaged SU-8 structures when they it will remain as part of the device.

The entire process was optimized for our specific application beginning with the layer thickness required.

Actually, we didn't need a thick layer of SU-8. We tried to optimize the attachment of SU-8 to the Si waveguides, so we needed a not too viscose thin layer . After observing the table at figure 4.2, a dilute SU-8 2 was chosen. The concentration was 50% of SU-8 2 and 50% SU-8 developer.

Product Name	Viscosity (cSt)	Thickness (µms)	Spin Speed (rpm)
		1.5	3000
SU-8 2	45	2	2000
		5	1000
		5	3000
SU-8 5	290	7	2000

Figure 4.2: Thickness vs. spin speed data for selected SU-8 resists.

The following step was chosen the speed of the **spin coater** to spread the layer of SU-8 over the sample. After many tests using different speeds, and then measuring the thickness with the Thalystep machine, we conclude that the speed and the time for the spin coater would be 6000rpm (revolutions per minute) during 40 seconds.

Using these parameters, the thickness obtained was 350 nm, a thickness that we consider suitable for our application. Afterwards, every step should be optimized.

The **soft bake** after the spinning of SU8 was necessary. Following the guidelines about how to use the product provided by MicroChem [11], the sample would be baked on a hot plate at 65^oC during one minute, and one minute more at 95^oC.

Product Name	Thickness (µms)	Pre-bake @ 65°C	Softbake @ 95°C
	1.5	1	1
SU-8 2	2	1	3
	5	1	3
	5	1	3
SU-8 5	7	2	5

Figure 4.3: Recommended soft bake parameters.

SU-8 is optimized for near UV (350-400nm) **exposure**, hence, 10 seconds of exposure at 365nm were chosen as exposure parameters for this determined thickness. This parameters were decided after some experimentation with the samples. This step, and the followings are explained in next subsection 4.2.2 Lithography in order to follow the real progress of the process.

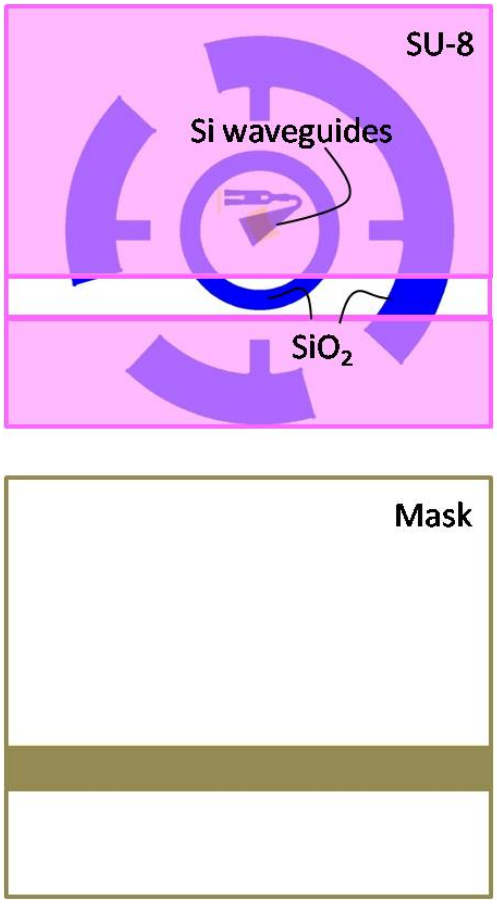

Figure 4.4: Exact position of the required aperture in SU-8.

Product Name	Thickness (µms)	PEB 1 @65°C	PEB 2 @95°C
	1.5	1	1
SU-8 2	2	1	1
	5	1	1
	5	1	1
SU-8 5	7	1	1

Figure 4.5: Recommended post exposure bake parameters.

4.2.2 Lithography

Looking at the general sketch of the process in figure 4.1, the third step is the HF underetching, that will remove the layer of SiO_2 from the sample. To achieve this, an aperture in the SU-8 layer was required.

Contact lithography was used to make this hole in the SU-8 layer. A specific mask was used to locate it at the proper position on the chip. Figure 4.4 illustrates the exact position of the required aperture. Assuming that SU-8 is a negative photoresist, the mask used during the lithography was exactly the negative part of the SU-8 left. It is also shown at the same picture. As a result of the exposure at 365nm during 10 seconds, the aperture was clearly defined over SU-8 layer.

The next step was the **post expose bake**, that was determined by means of the tables provided by MicroChem. Again, one minute at 65^oC and another one at 95^oC were the parameters for the post exposure bake.

Development with MicroChem SU-8 Developer improves the quality of the resist. The sample was immersed during one minute in SU-8 Developer, then it should be rinsed with isopropyl alcohol (IPA), and dried with a gentle stream of nitrogen.

The controlled **hard bake** is recommended after development, hence, the sample was on a hot plate at 200^{o}C during 10 min.

The SU-8 treatment ends here. Now the third step of the general process is explained.

4.2.3 HF etching

HF etching is the next step. It consists of the immersion of the sample in HF to remove the SiO_2. This immersion was carefully controlled, checking how the HF was advancing through the aperture made. Pictures in figure 4.6 show this progress after 15 min, 30 min and 35 min of immersion. It's visible as a double line that was progressing with time around Si waveguides, until our structure was completely surrounded by it. After 35 min the microrings and grating couplers were completely underetched, then, the sample was rinsed with water and dried. After this step, our structure was ready to be stuck to the fiber.

Figure 4.6: HF progress. Pictures after 15 min, 30 min and 35 min of HF immersion respectively.

4.2.4 Alignment and curing

The alignment of the fiber above the grating couplers is a difficult procedure due to the fact that the same fiber is used to couple light in and out. Therefore, a small error in the alignment will affect the signal twice. The alignment is optimized by moving the fiber with the XYZ actuators without forgetting also to optimize the angle of the sample stage, until the power detected by the power meter is maximized . This part of the setup can be seen in pictures 4.7 and 4.10. Figures 4.8 and 4.9 illustrate the position of the rings on the sample and the described angle to be optimized.

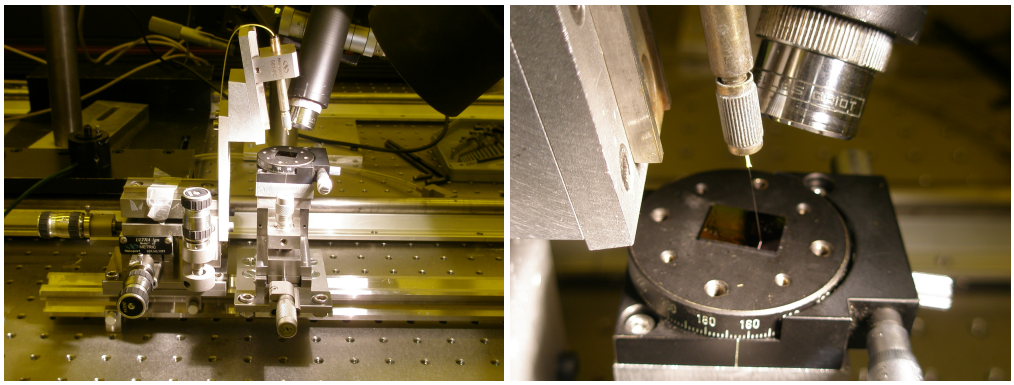

Figure 4.7: Alignment setup

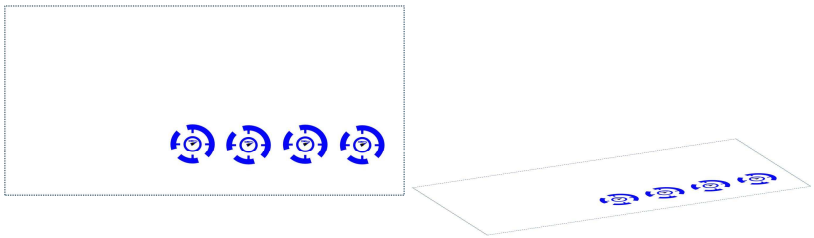

((a)) Four rings on the sample ((b)) Real position to measure

Figure 4.8: Position of rings on the sample

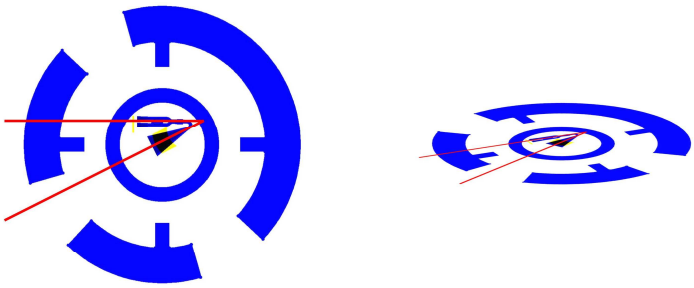

((a)) Ring on the sample ((b)) Real position to measure

Figure 4.9: The angle to be optimized is the angle described between the red lines

In the same way, the polarization can be set to TE by manually changing the polarization controller until the detected power is maximal. The alignment is done with the fiber at a safe vertical distance from the sample. The fiber is brought closer to the sample vertically, so that the fiber and its shadow appear on the screen. The grating coupler, which should be visible at the beginning of the alignment, is positioned between the edges of the fibre and its shadow, and then the fiber can be moved closer to the sample to optimize transmission.

Pictures in figure 4.10 show the screen of the monitor, when the alignment is being done.

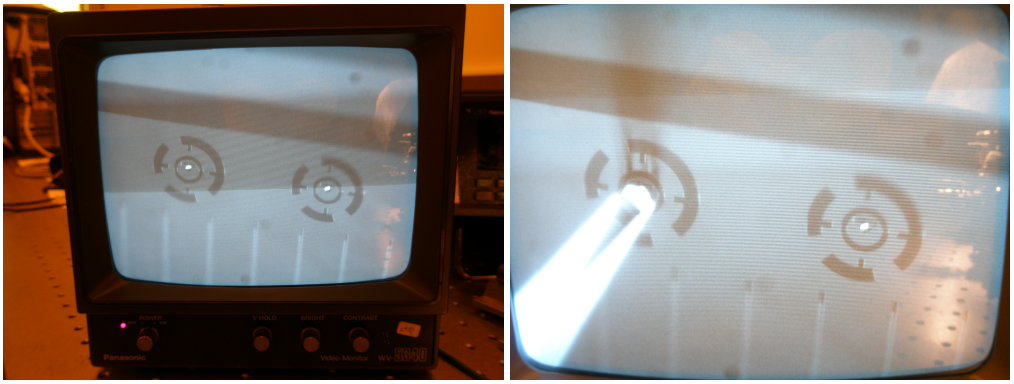

((a)) Microrings focused. ((b)) Fiber and its shadow during the alignment.

Figure 4.10: Monitor screen during the alignment

At this point in the process, the alignment was not active yet. Just a fiber, without light source connected, was used to do the first tests of this step. The alignment was only visual, with the camera and the monitor, and SU-8 was used like a glue to stick the fiber to the chip.

A small drop of SU-8 wetted the tip of the fiber with a short contact between them. Thus, the fiber had a very small drop in its tip that was deposited above our structure after a delicate alignment. The curing of this drop of SU-8 was performed by the UV lamp during 3 min.(See 4.11)

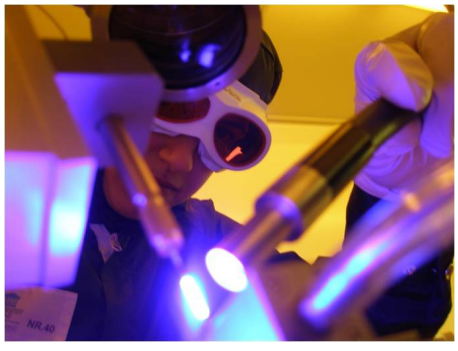

Figure 4.11: Curing

After this procedure, our structure may be stuck to the tip of the fiber. Following pictures show first results after pull up the fiber.

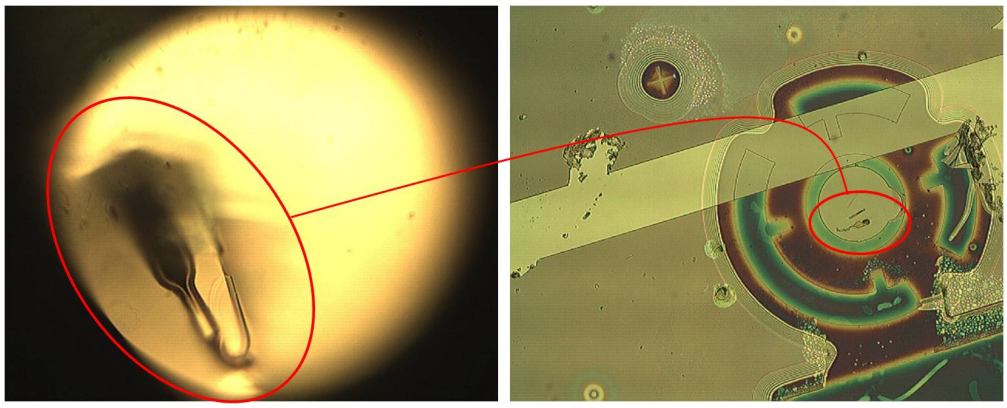

Figure 4.12: Tip of the fiber after the sticking process and what is left on the sample. First try.

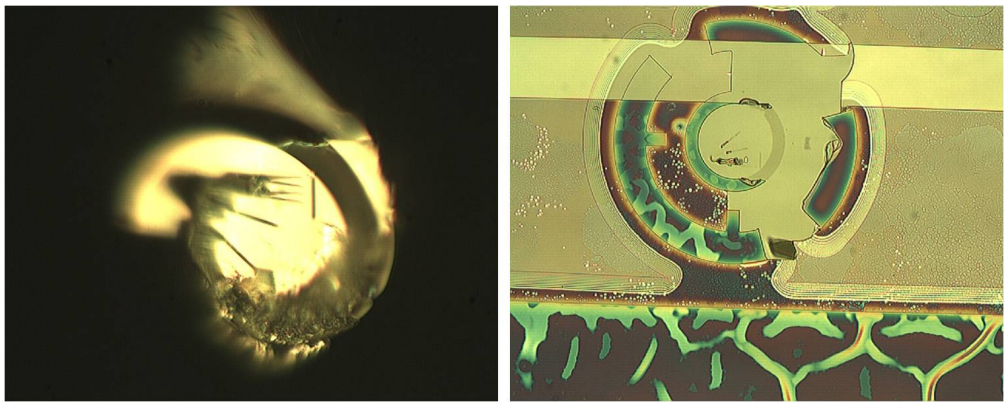

Figure 4.13: Tip of the fiber after the sticking process and what is left on the sample. Second try.

Pictures show the tip of the fiber after the sticking procedure and the corresponding ring on the sample where it has been stuck. It's appreciable that the first sticking results were not good. Parts of our structure were still on the sample, and the fiber tip had just picked up some broken elements.

At this point of the process, it was the right time to optimize it. This part will be explained in the next section Development.

4.3 Development

This section will describe each change of the original process to achieve an improvement, and how difficulties were coming up in the progress of the process.

4.3.1 Sticking Optimization

After first attempts, the sticking of our structure wasn't good. We improve this point by optimizing the hard bake. The sample was on the hot plate at 95^{o}C, and the temperature was increasing until 170^{o}C during 10 min. Results were much better. See figure 4.14

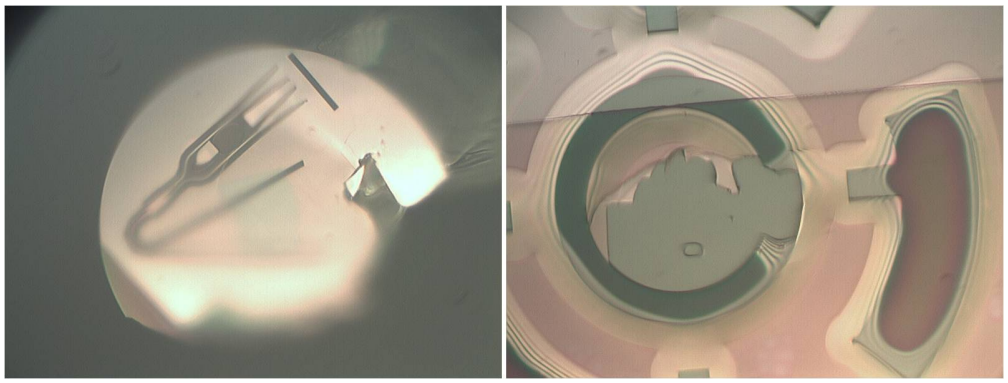

Figure 4.14: Improvement after optimizing hard bake.

The SU-8 thickness layer was also optimized. After some tests with different speeds for the spin coater, 3000 rpm during 40s were chosen as parameters, obtaining a layer of 440 nm of SU-8. Results also improved. See figure 4.15.

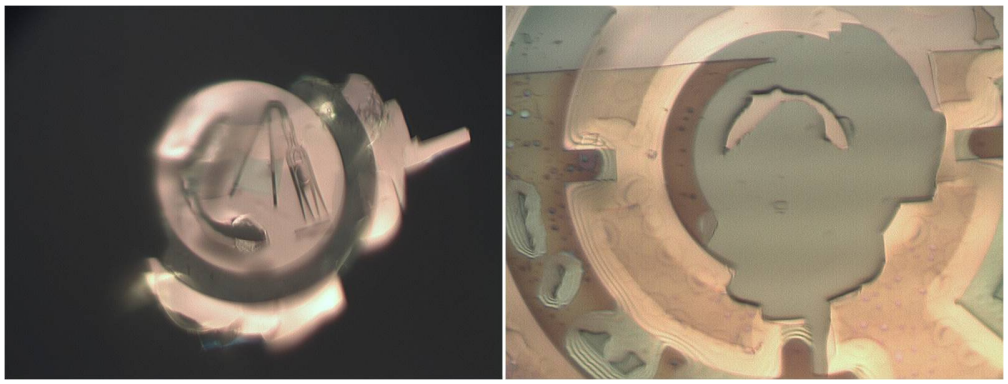

Figure 4.15: Improvement after optimizing SU-8 layer thickness.

The rest of parameters of the process were stable, so we couldn't optimize any other parameter. Results had improved, but they weren't good enough.

A new approach was proposed to try obtain better results.

Firstly, an adhesion promoter was applied over the sample before SU8, to try to improve the attachment of Si waveguides to the fiber. Results weren't better.

Secondly, BCB was proposed to replace SU-8, but in the HF undertetching step, BCB didn't resist 35 min of immersion. At figure 4.16 it's possible to see that BCB layer is detached from the sample, even pulling off part of our structure. Red lines show where the BCB was before the underetching.

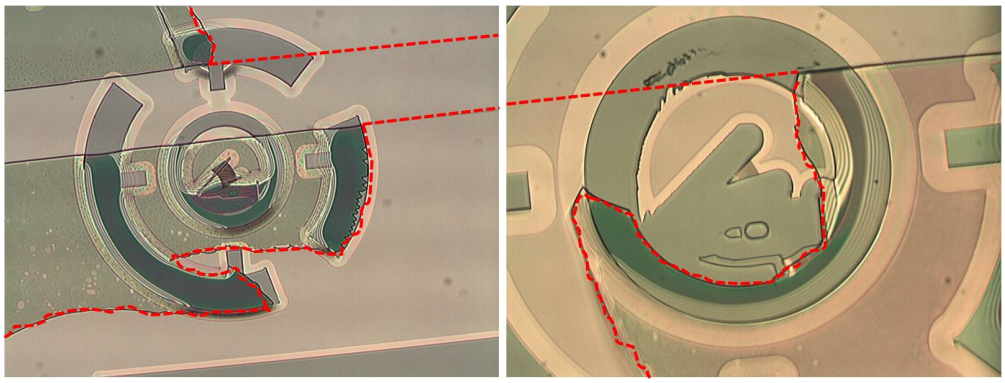

Figure 4.16: BCB detached from the sample.

The idea of replacing SU-8 was rejected after observing these results, but a new thought about the conditions of the original sample was developed.

The possible native SiO_2 created on the surface of the sample would be removed after the HF immersion, and consequently the attachment of SU-8 to Si waveguides was bad. Figure 4.17 illustrates the impossibility of the sticking of the Si waveguides to the SU-8 after HF underetching.

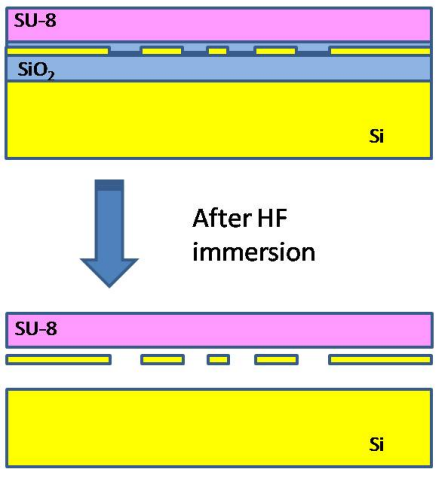

Figure 4.17: Conditions after HF underetching. Bad sticking.

To solve this problem, a new step was added to the process. Before applying SU-8 over the sample, it was introduced into HF during 5 s in order to remove the possible layer, as much 2 nm, of native SiO_2.

Results are shown in the next pictures. Our structure is completely stuck to the fiber.

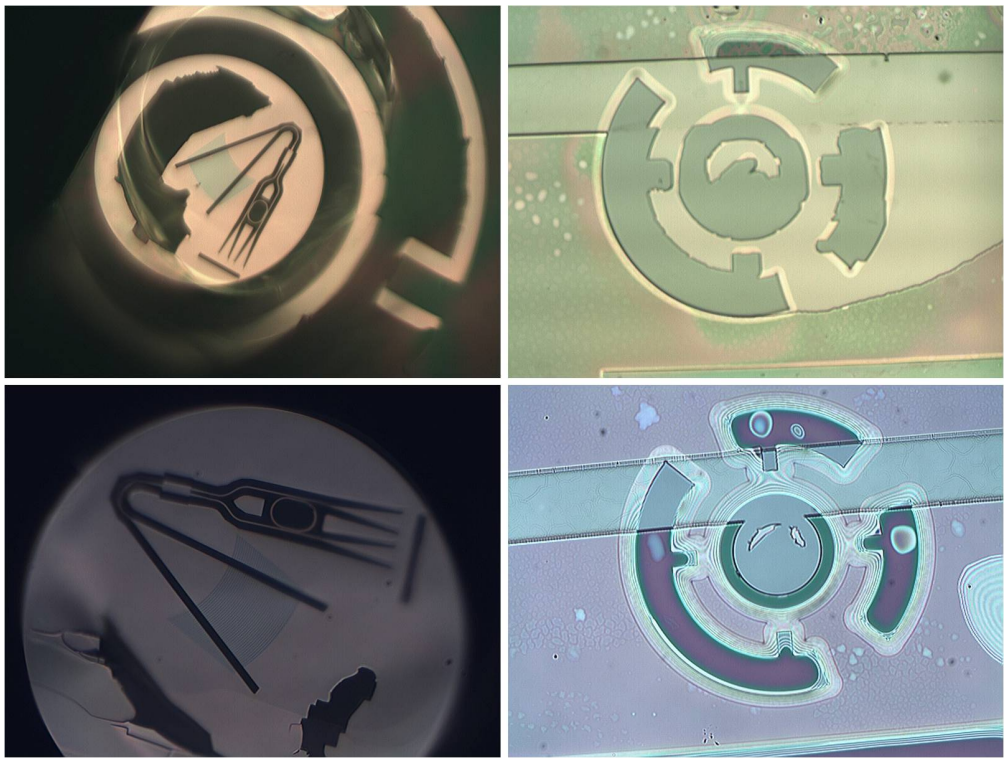

Figure 4.18: Fiber tip and sample after sticking procedure. Improvement after previous HF dip

Problems associated to the physical fabrication were solved. The process was ready to incorporate the active alignment required for our application.

4.3.2 Active alignment and detection of the signal

In order to have a clear vision of the process at this point, we briefly review it here.

1. HF dip during 5 s.
2. SU-8 layer
3. Lithography
4. HF underetching during 35 min.
5. Alignment and curing.

After doing 4 steps of the process, the alignment was the next step. The active alignment was performed as explained in subsection 4.2.4, Alignment and curing. A tunable laser was used as source light following the description of the measurement setup in last chapter. (See section 3.1). The tip of the fiber was wetted by a small drop of SU-8 used to stick the fiber to the chip.

The first problem found was the fast solidification of the small SU-8 drop. This solidification was due to the heat that the light provoked when it went through the fiber. The alignment required a long time to find resonances, and SU-8 was cured almost immediately. Another glue was needed to replace SU-8. PAK was proposed as solution. Again, some tests were required to be sure that PAK was proper. Results, shown at figure 4.19, were also good.

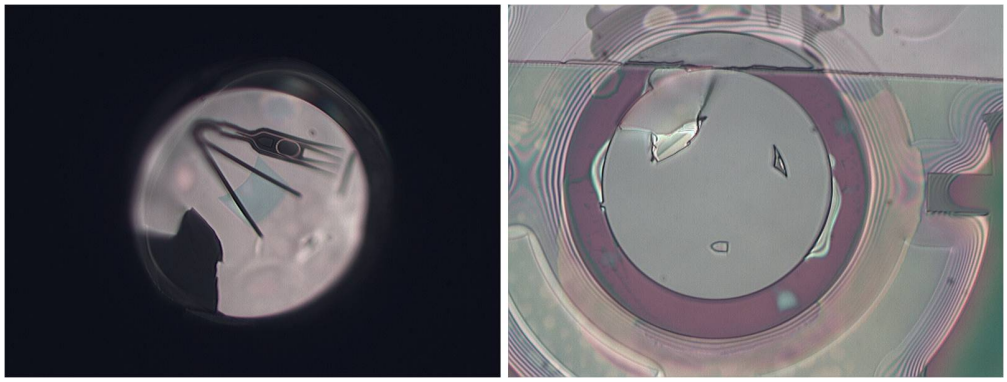

Figure 4.19: Fiber tip and sample after sticking procedure using a drop of PAK as glue

Once known that the procedure of the alignment was possible following the last steps, the detection of the resonances during the alignment was the next challenge. To ensure that the detection was possible and successful, the search of this resonances was performed after each step of the treatment over the sample. Figures 4.20, 4.21, and 4.22 show graphs with the detected resonances after each step.

Resonance wavelength shifts between each graph are owed to the change of the environment of the ring after each step. Thereby the effective index changes caused these shifts.

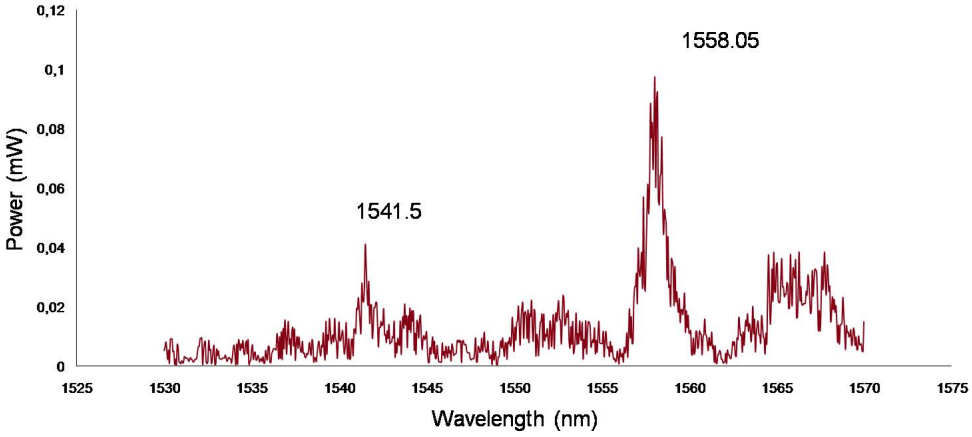

Figure 4.20: Original Sample

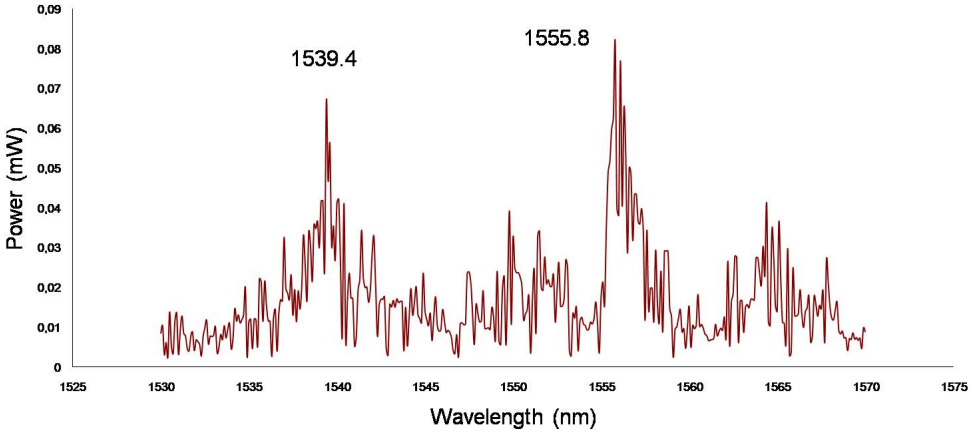

Figure 4.21: Detected signal after first HF dip

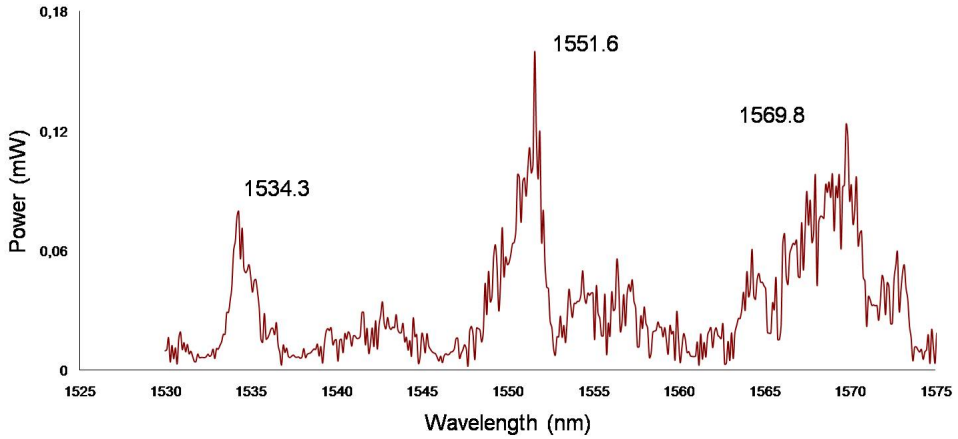

Figure 4.22: Detected signal after SU8 layer on the sample

Problems appeared again after the HF etching. Resonances couldn't be seen due to optical losses that had increased after underetching (See 4.23).

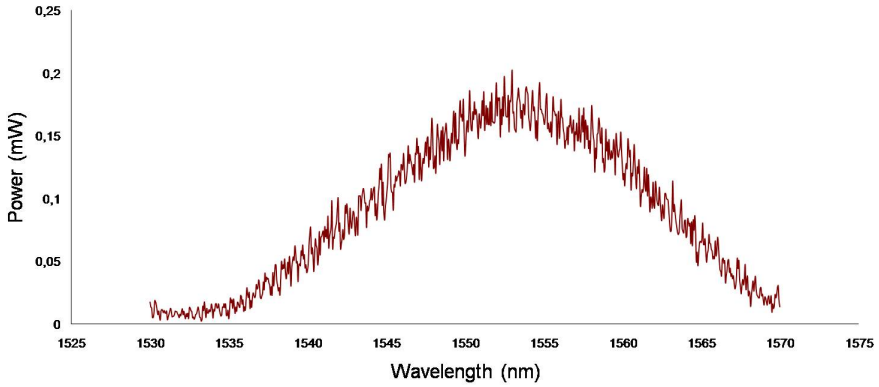

Figure 4.23: Detected signal after HF underetching, no resonances

Just once, the detected signal showed resonances. It can be observed at figures 4.24, where the detection was performed using PAK, and without PAK, to ensure that PAK wasn't the problem.

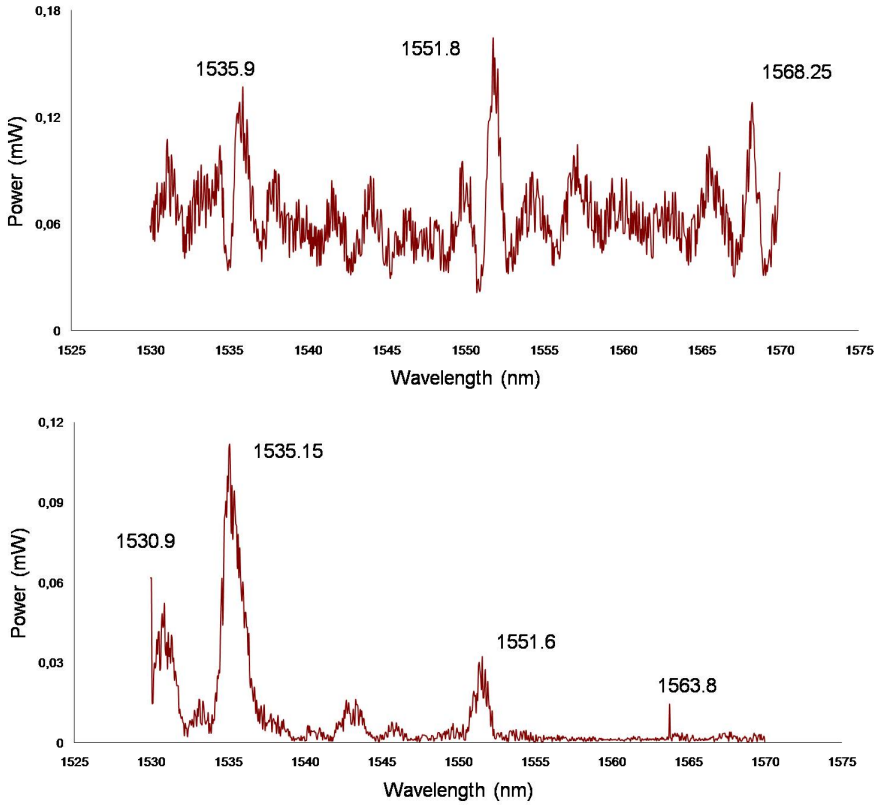

Figure 4.24: Detected signal after HF underetching, without and with PAK, respectively.

4.3.3 Research

In order to find the reason of the problem after the HF underetching, an investigation about waveguide conditions after being exposed to HF began. Two samples with 440 nm and 1μm of SU-8 layer on them were underetched as it was done before with all the rest of the samples, however, no lithography step was done on them. Pictures at figure 4.25 show the cross-section of one of this samples. The HF effects over the sample are appreciable.

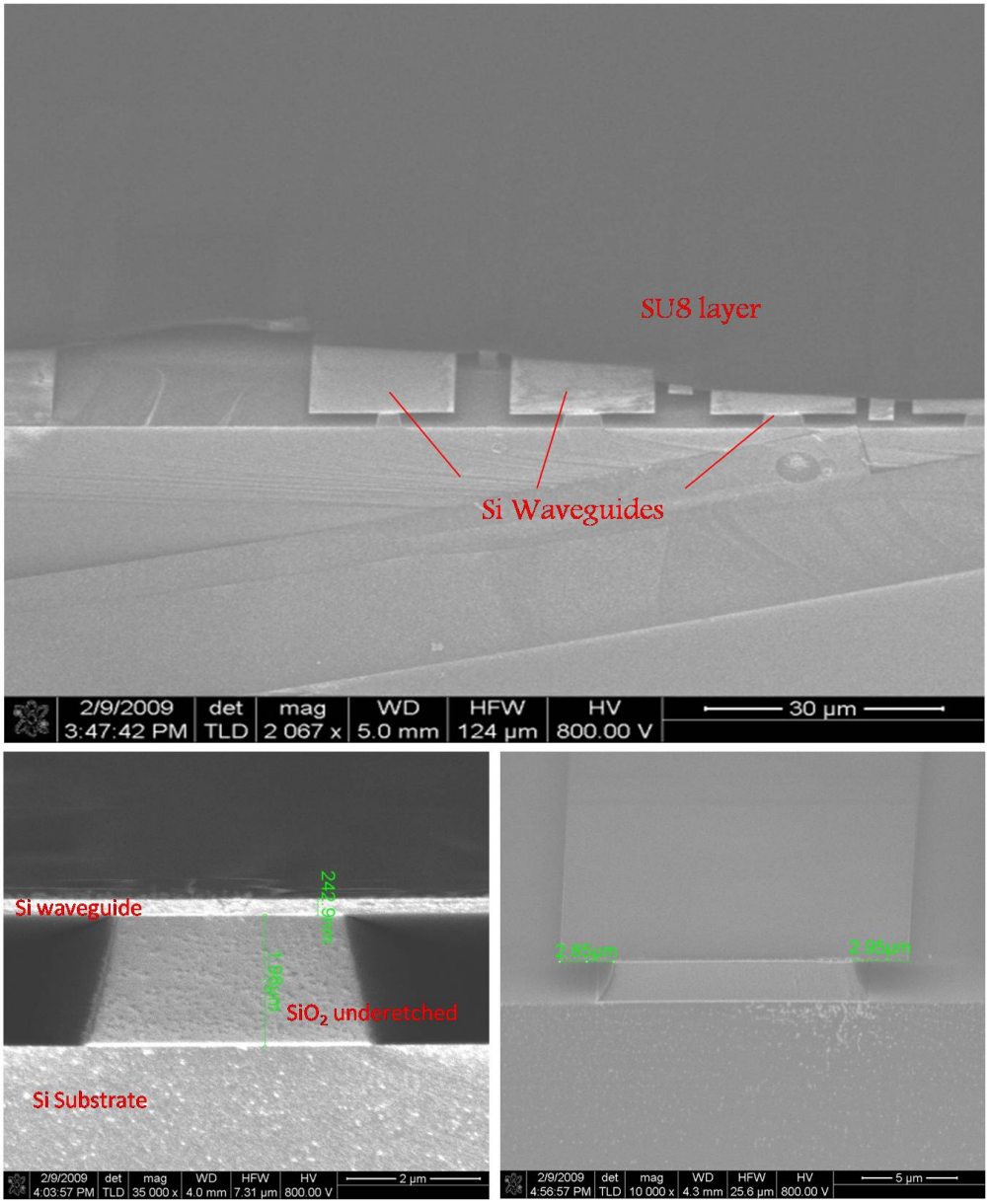

Figure 4.25: Cross-section of a sample. Waveguides condition

These figures are pictures taken by a Scanning Electron Microscope (SEM). In them it's possible to differentiate the Si waveguide (220 nm) and the part of SiO_2 that stays after the HF exposition (2μm). Indeed, waveguides were exposed to HF for too long, such that HF could go through the SU-8 and underetch the sample.

In order to solve this problem, we decided to modify the etch process and after some research about which products were able to underetch SiO_2 without affect Si waveguides, buffered HF was proposed as solution:
$[BOE] = (NH_4F) + (HF)$.

Buffered HF was analyzed checking if it went through SU-8 and underetch the sample even without any lithography step. Results were not satisfactory. Three hours were required by BOE to underetch the SiO_2 of our sample. During this long time, SU-8 was slowly destroyed, and consequently, the following step in the fabrication process didn't work. It can be seen in the next pictures.

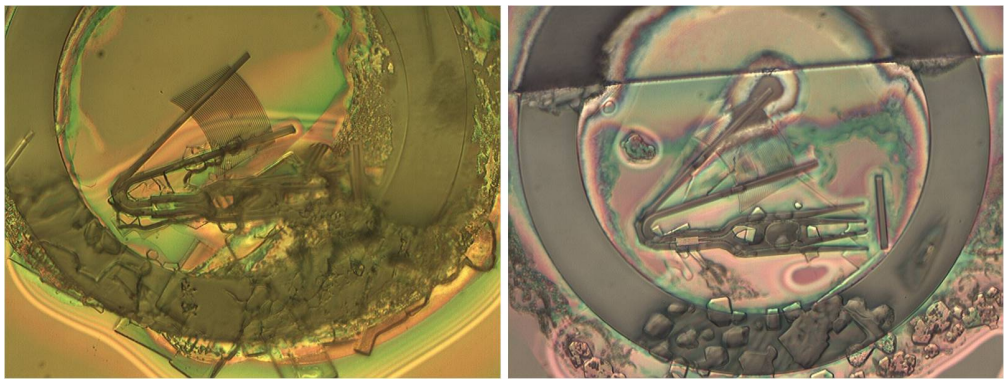

Figure 4.26: SU-8 destroyed after 3 h in BOE.

The failure of BOE wasn't expected, and the only line of investigation was to analyze again problems with HF. We arrived to other conclusion: actually, waveguides didn't seem damaged, despite the exposure to HF during 35 min. In this study we found a possible reason about why we couldn't find resonances after HF underetching.

Pictures of figure 4.27 show a cross section of the grating couplers of two different samples after the HF underetching. Grating couplers weren't damaged, but at first picture, the inclination of them is clearly appreciable. Between grating couplers and Si substrate, air replaced SiO_2 as we expected. At second picture, there is nothing between grating couplers and Si substrate, it's

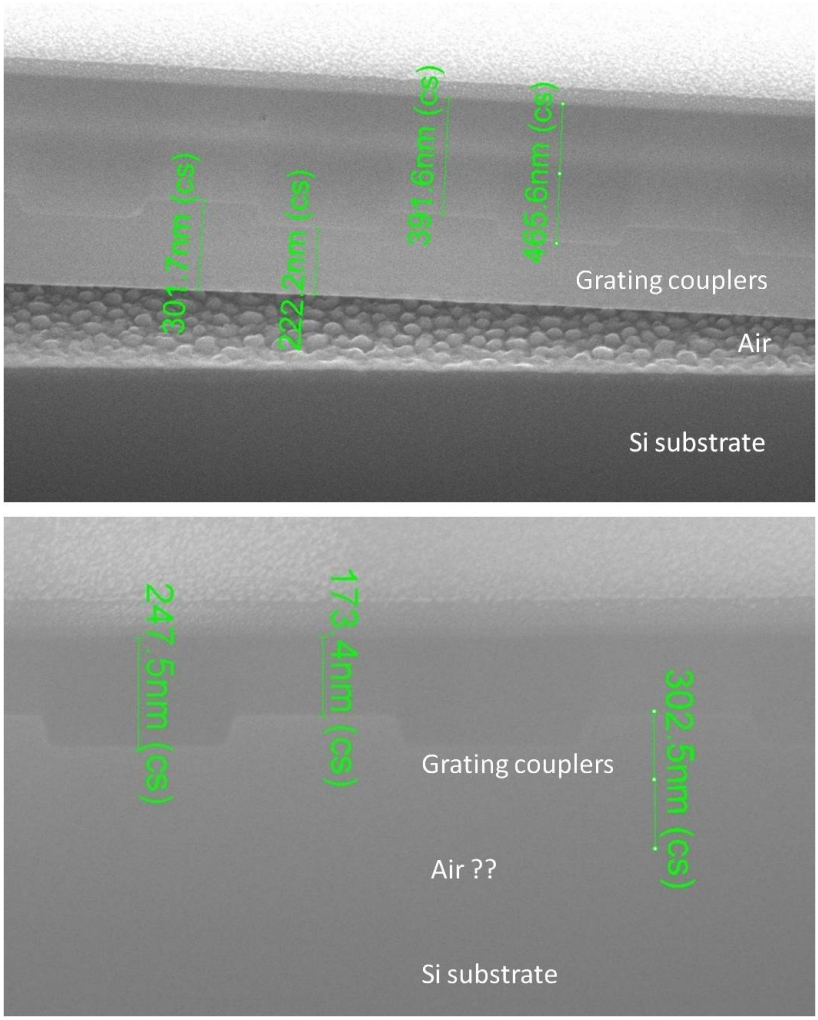

Figure 4.27: Our structure was collapsed after HF underetching.

not possible to see the difference between them, because they both are Si. Our structure was collapsed.

4.4 Conclusions and perspectives

A deep analysis about the progression of this process has been described in the last sections. Final results prove that the detection of resonances after the HF underetching was almost impossible after the collapse of the structure.

A possible explanation about why once resonances where detected after this critical step, is that the glue used to stick the chip to the fiber, went underneath the structures, providing the required change in the refraction index. However, in this case, it was not possible to stick the the chip to the fiber after

pulling it up, because the PAK underneath was also cured, and didn't allow to pull out the structure.

To avoid this collapse, different thickness of the layer of SU-8, 440 nm, 1 μm, 2 μm, and 3 μm, were tested unsuccessfully. The sticking wasn't bad, but no resonance could be found.

A possible solution would be find the optimum thickness of the SU-8 layer that hold the structure and avoid the collapse. To find out this thickness, many experiments and the availability of SEM during a lot of time and would be required. The idea of a new process was considerate, thinking that it would be a easier way to obtain good result. Nonetheless, the mentioned optimization could be developed in the future.

Chapter 5

Process 2: Etching after sticking.

This process was developed in order to avoid the collapse problem of process 1. It consists of the same five steps of the process 1, but changing the order of the two last steps. An overview of the process is illustrated in the following picture.

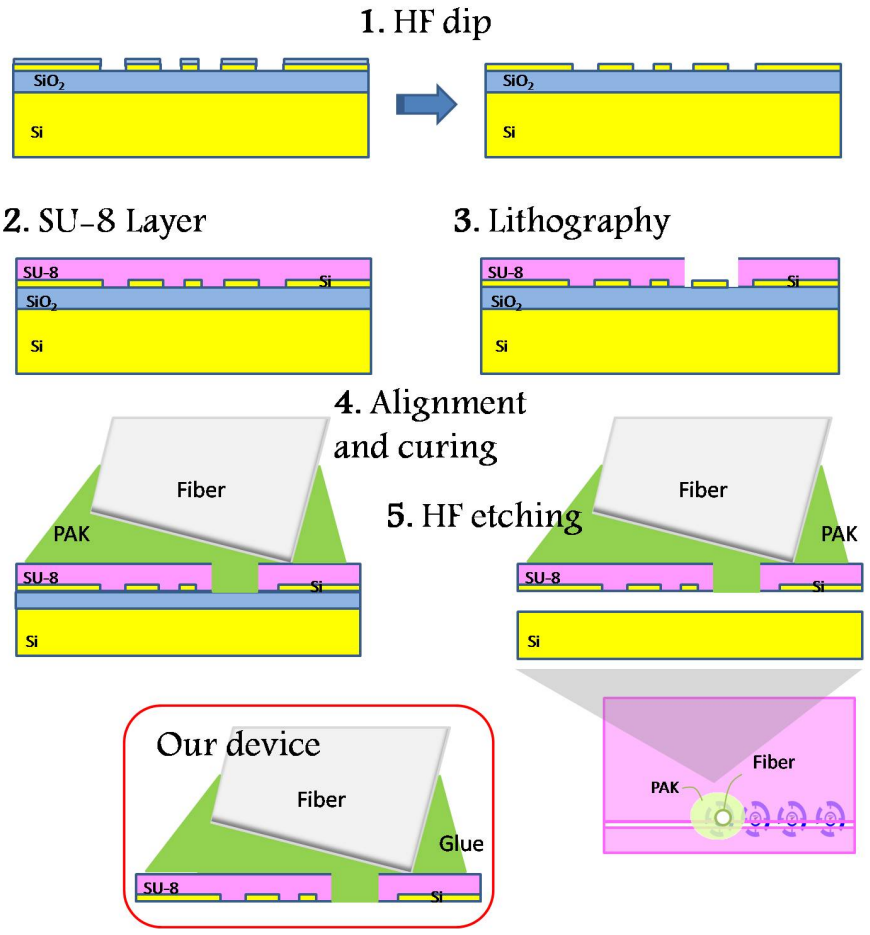

Figure 5.1: General sketch process 2.

5.1 Process

Steps of this process are exactly the same steps of process 1. Just some changes will be explained in this section.

After the HF dip, an SU-8 layer was applied over the chip. Now its thickness was 3 μm, which was decided after a successful sticking test.

The alignment and curing were not changed, but there was something that we should consider. After this step, the sample and the fiber should be introduced into HF. Optical fiber in HF wouldn't resist without protection. For that reason, the fiber had to be protected with several layers of SU-8 before align it.

Problems appeared at this moment. After the curing, the fiber holder should be transported from the measurements room to the chemical bench in the cleanroom. The fiber should hold the sample stuck to it by means of the small drop of PAK cured. However, this small drop of PAK couldn't hold the entire sample.

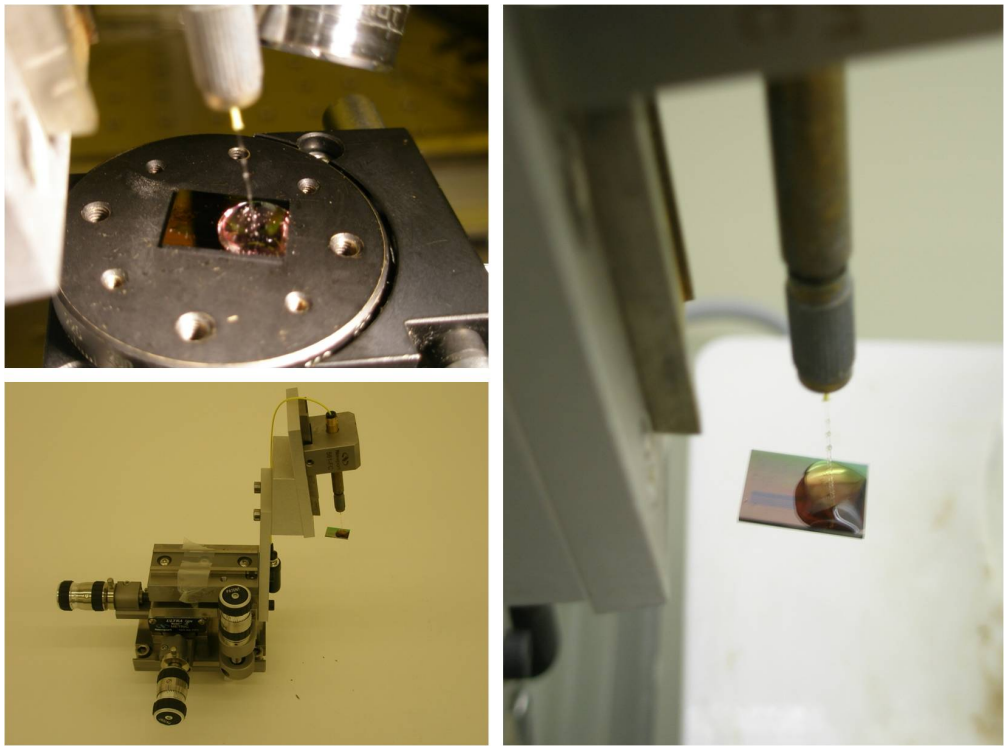

Figure 5.2: Big drop of PAK

The solution was to use a big drop of PAK deposited on the sample to do the alignment. Pictures at figure 5.2 illustrates the big drop of PAK required

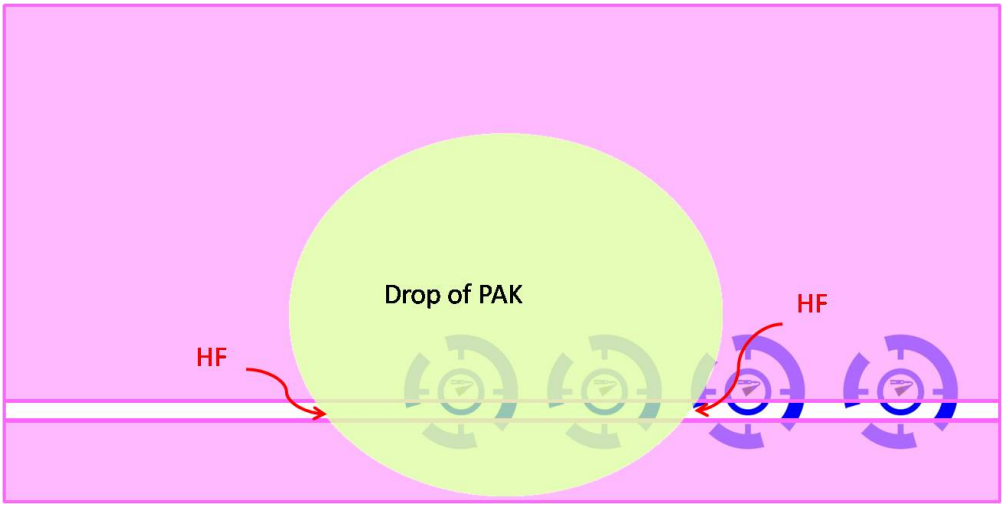

Figure 5.3: Big drop of PAK

and how the fiber and sample were transported in order to do the HF underetching.

Consequently, another problem came up. The HF underetching took a long time to remove the SiO_2 below our structure due to the big drop of PAK had filled the aperture in SU-8 previously done by lithography. At figure 5.3 it's visible that the underetching began really far from our structure.

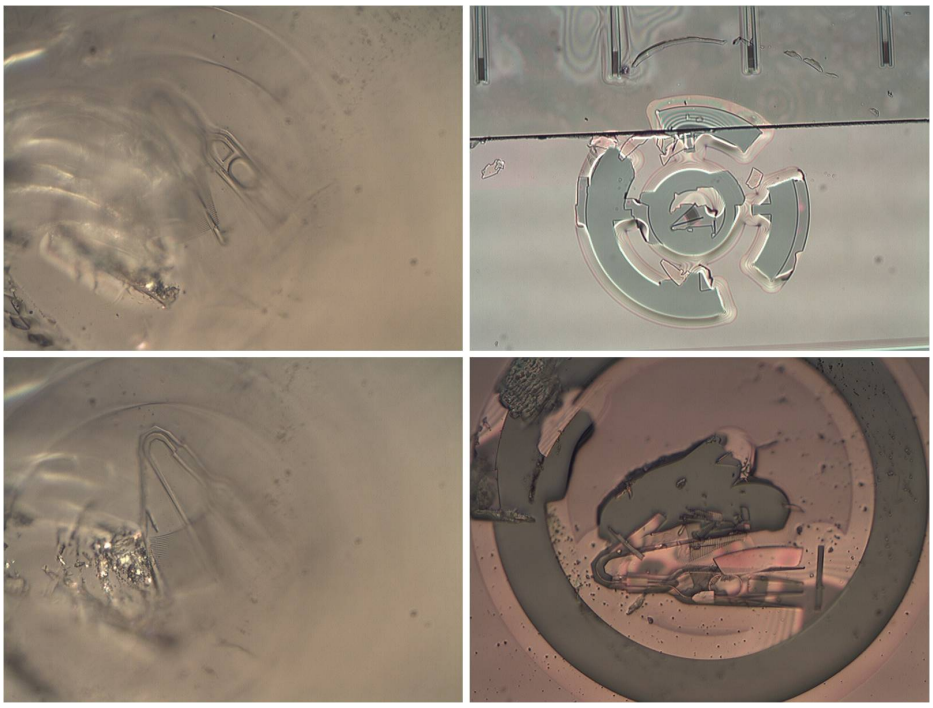

Figure 5.4: Fiber and sample after underetching using PAK

After 3 hours of underetching , the adhesion of PAK and SU-8 was really damaged. Results after some tests are shown in figure 5.4.

It is possible to see on the fiber tip a shape of our structure, but there were not waveguides, it was just the trace. On the samples, some parts of our structure were still there.

An alternative was to use again a drop of SU-8 to do the alignment. Problems that we had with the first process about the fast solidification of SU-8 didn't appear, because the drop was now bigger.

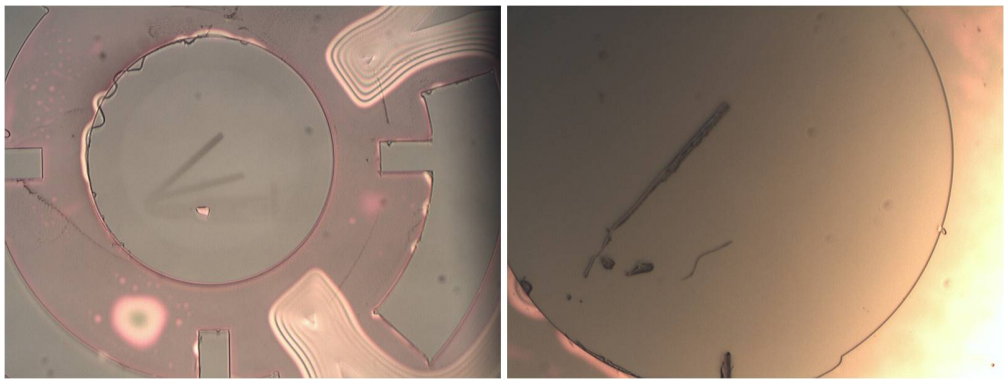

Figure 5.5: Fiber and sample after underetching using SU-8

However, results after underetching weren't good. It took a shorter time, but enough to damage the adhesion between fiber and sample.Results were similar.

Pictures 5.5 show that rests of the structure were still on the sample. The same process was tried with different thickness of the SU-8 layer, but no improvement was obtained.

5.2 Conclusions and perspectives

We showed that this process couldn't provide the desired results. The uncontrolled size of the drop of PAK was a important inconvenience. This size could be controlled using another mask to make some others apertures in the SU-8 layer. A possible sketch of this mask over the sample is shown in figure 5.6

The first aperture done near the rings could control the size of the drop, allowing the HF underetching by means of the second aperture. A redesign of the chip would be also necessary, to add SiO_2 where the apertures would

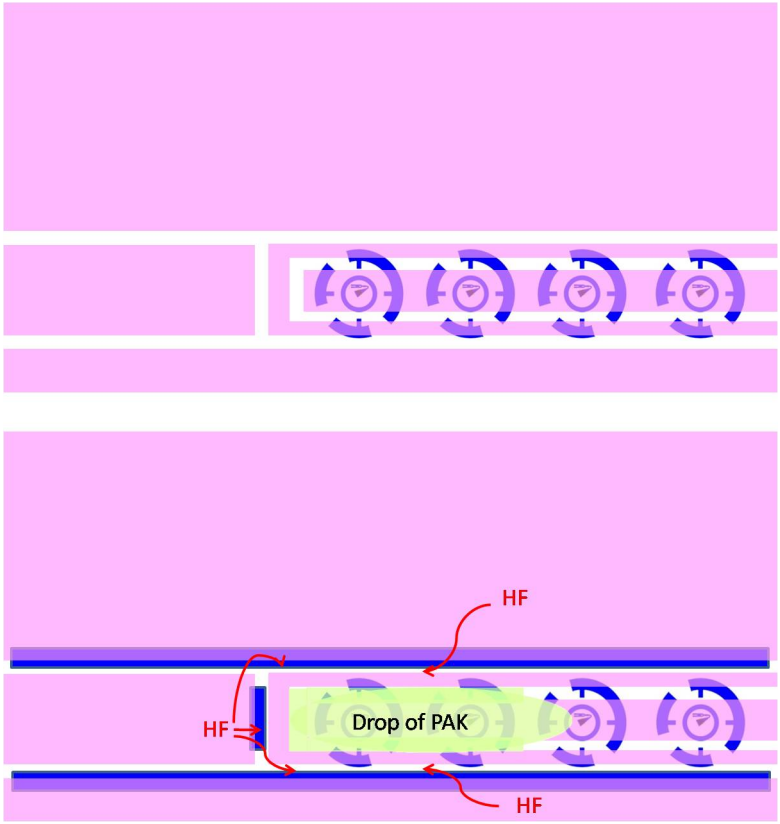

Figure 5.6: Possible sketch for a future mask

be done. The time required to redesign the sample and the mask would be an inconvenience for the development of this thesis, but it could be an idea to be tried in the future.

A new process, completely different from the processes already explained, was considered to try to obtain some results. It will be explained in chapter 6 Process 3: Removing Si substrate and SiO_2

Chapter 6

Process 3: Removing of Si substrate and SiO_2

This process was performed as last alternative to obtain some good results. Last tried processes could provide good results, but time and resources required to achieve them were unacceptable for this thesis. The idea of this new

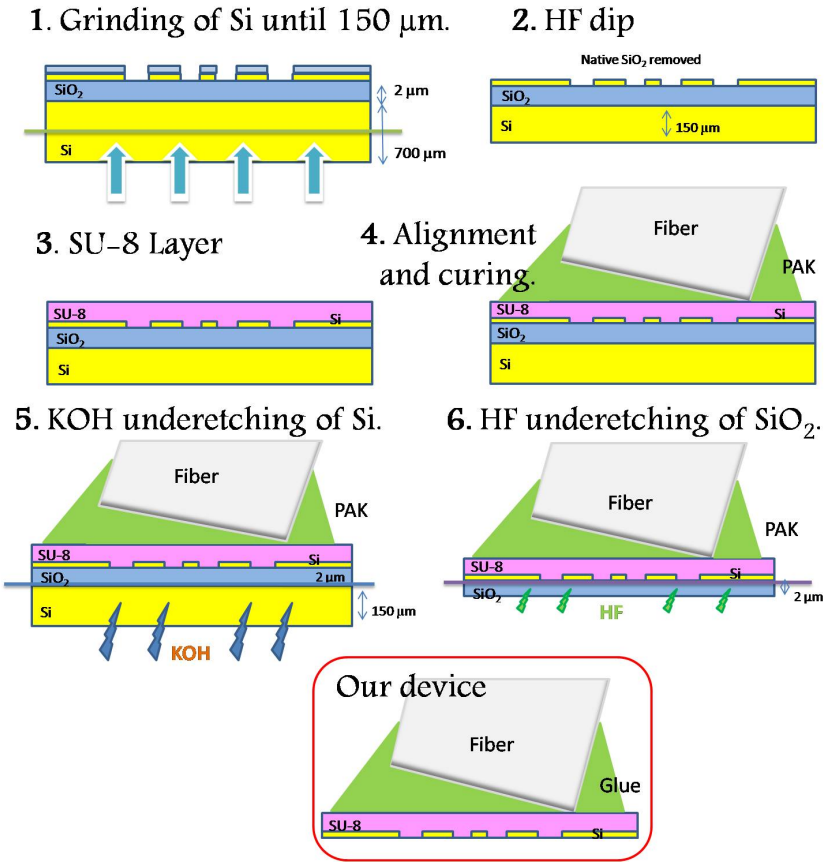

Figure 6.1: General sketch process 3.

process was very different from last processes, but it was quickly accepted and developed. The sketch that illustrates the first idea of this process is shown in figure 6.1.

The main idea was to remove each layer of the chip from the bottom, in order to leave just the Si waveguides stuck to the fiber. This process consists of six steps that will be explained at next section.

6.1 Process

6.1.1 Grinding

The first step of this process is the grinding of part of the Si substrate. The original Si substrate thickness is 700 μm, and we tried to reduce it to 150 μm during approximately three hours of grinding. This Si thinning was done by means of a polishing machine, using a solution of SiC (silicon carbide) powder in water. Before grinding, the sample was fixed on a glass plate with wax heated at 150^{o}C. After this three hours, it could be released from the glass plate and cleaned with boiling TCE (trichloroethylene), acetone, IPA (isopropyl

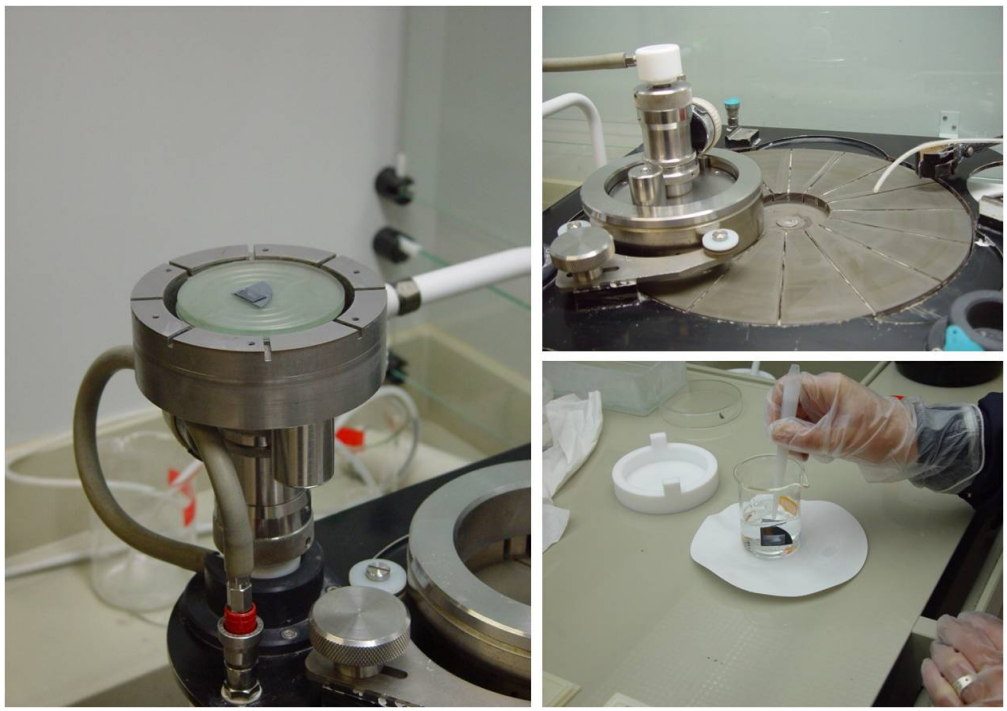

Figure 6.2: Grinding. [5]

alcohol) and water. This cleaning procedure required high delicacy because the chip was very thin and fragile. Picture 6.2 illustrates this process.

Now, the sample was ready to undergo the next steps.

6.1.2 HF dip, SU-8 layer, alignment and curing

The next three steps have been already explained in last chapters. Anyway, a short review is given in this section.

Firstly, the HF dip consisted of the introduction of the sample into HF during 5 seconds, in order to remove the possible native silicon created on its surface. This avoided the bad sticking of SU-8 layer to Si waveguides, one of the problems of the first process.

Secondly, SU-8 layer was applied over the chip. The thickness of this layer was also discussed in the first process, where the optimization of the sticking step, fixed a range of possible thicknesses from 440 nm to 3 μm.

Thirdly, the alignment was performed in the measurement setup described in chapter 3, Fabrication and measurements. PAK, was again used as glue, to stuck the fiber to the sample.

Similar to process 2, the fiber was coated with several layers of SU-8 to protect it from the followings steps, where it would be exposed to HF, and in this process, also to KOH.

Once the alignment and curing was finished, the delicate transport of the fiber and sample to the chemical bench in the cleanroom was necessary to do the next step, the underetching.

Concerning the alignment, it still wasn't active because we wanted to be sure that the physical fabrication was possible.

6.1.3 KOH and HF underetching

The KOH underetching was done by introducing the sample, and inevitably part of the fiber stuck to it, into KOH. The KOH solution was prepared with 20% concentration, 30 g of KOH, dissolved in 120 ml of water. The temperature was fixed and carefully controlled at 75^{o}C, at which the theoretical rates of the underetching of the Si were approximately 1 μm/min.

The thickness of the Si substrate of our sample was 150 μm after the grinding, therefore the underetching duration should be 150 min. Problems appeared at this point, but they will be explained in next section 6.2 Develop-

ment, where we will talk about each problem that are arisen, and how we tried to solve them.

After removing all the Si substrate of our sample, just Si waveguides and SiO_2 would be left. The last step, HF underetching, would remove the 2 μm of SiO_2, in order to obtain our device, Si waveguides stuck to the fiber. Considering theoretical rates, approximately 1,8 μm/min, sample and fiber should be into HF less than 2 minutes.

Actually, this last step was never carried out, because problems with KOH didn't allow us to arrive at this point. The next section will detail all these problems.

6.2 Development

We came up with different ideas were coming up to try to resolve the difficulties found during the progress of the process. This difficulties arose during the fifth step, KOH underetching.

6.2.1 PAK and SU-8

Sample and fiber should be into KOH, during approximately 150 min. PAK was used in the sticking of the fiber, and then sample and fiber were introduced into KOH. After one hour there, the sample fell from the fiber, and began to be dissolved in KOH. It was tried again, now, observing carefully the sample and fiber to try to find out why sample had fallen. The conclusion was that PAK came unstuck after one hour into KOH, hence, the sample fell.

SU-8 was proposed to replace PAK in the alignment, however, its use was also unsuccessful. As well as PAK, SU-8 came unstuck, but this, after 90 min into KOH. The SU-8 used was SU-8 2, the less viscous SU-8 of the range. Another try with SU-8 10, more viscous, was carried out. The sample resisted longer time, but not enough, it also fell.

6.2.2 ICP

The first idea to solve this problem was to add a new step. It should be between the application of the SU-8 layer over the chip and the alignment. It was the use of the ICP (inductively coupled plasma) etch system to thin the Si a bit more before the KOH underetching.

The objective of this new step was to reduce the thickness of the Si substrate and moreover the time required to underetch it in KOH.

The sample could resist 50 min in KOH using a drop of SU-8 10 during the alignment, and then, we would need to underetch Si in ICP until 50 μm. To achieve this, the time required in ICP would be 2 hours approximately.

The sample was introduced the ICP, after SU-8 was applied over the sample. The first try was just during 30 min, just to control how fast the Si substrate was being etched. The sample was carefully analyzed, and results are shown in pictures at figure 6.3. In them, it is easy to see that the corner of the sample, and our structures, quite near to the corner, are damaged after 30 min. Moreover, the SU-8 layer had disappeared.

Figure 6.3: Waveguides damaged after 30 minutes in ICP.

The first thought was to protect waveguides and SU-8 in ICP by means a photoresist. AZ 1505 and AZ 5214, were used with this intention, but results were the same, Si waveguides were damaged.

Consequently, we decided to skip this step, and try to find other solution.

The proposal about grinding the sample until Si substrate was 50 μm was immediately rejected. The handling of the chip would be too difficult, and it could be broken very easily.

Another proposal was accepted, it is explained at next subsection.

6.2.3 WAX

The use of a black wax to cover the sample and the chip, and thus, protect the top and sides from the KOH, was a strong idea that we carried out.

PAK was again the glue used in the alignment and the sticking. Then, fiber and sample were transported where KOH underetching would be performed. The preparation of the wax required to heat it to 90^oC and mix it in TCE. When it was melted, it was applied over the sample covering also the fiber. This application was very delicate because the wax quickly solidified, and it was difficult to cover all of the sample and fiber without breaking their union.

Once done this, sample and fiber, both covered with wax, were introduced into KOH. Figure 6.4 illustrates how the wax was applied.

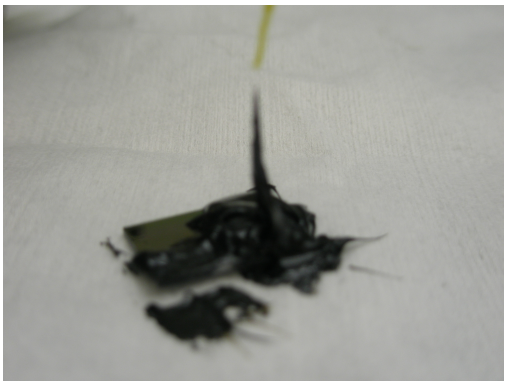

Figure 6.4: Applying wax over sample.

After short time in KOH, the wax was completely released from the sample, but just where the drop of PAK was. Consequently, after one hour our sample fell, similar to the last try. This step was repeated, but results were the same. The wax did not stick to PAK, therefore, there wasn't protection for PAK and sample.

Again SU-8 10 was proposed to replace PAK. After one hour, the sample also fell, because the wax was melting in the warm KOH gradually, and finally the sample wasn't protected.

To solve this new problem, a lot of wax was applied over the sample, in several times, this is, applying a layer and letting it solidify, and repeat it many times. Thus, any small hole allowed KOH to go under the wax and attacked the sample.

However, this thick layer of wax was't the solution. During the immersion, wax was also melting due to the high temperature of KOH, but, there was enough wax to protect sample, indeed, it resisted 150 min. The problem was that this melting wax was floating in KOH dissolving, and it also went underneath sample.

This fact made more difficult the underetching of the Si substrate and after 150 min into KOH, the sample didn't seem underetched at all.

Parameters to be optimized were checked. Temperature was controlled and even fixed at few grades higher, to accelerate the etching rate. Time of immersion was prolonged, 200 min. But any change in results was appreciable.

6.3 Conclusions and perspectives

The inevitable melting of wax during the KOH underetching turned out to be a great problem, impossible to be avoided. The research on other solution was interrupted by the lack of time.

However, a door for a future investigation was left opened. The research on a product that resists KOH, and protects SU-8, sample and fiber would solve our problem, providing as result our device.

Chapter 7

Conclusions and perspectives

The fiber sensor probe proposed in this thesis has turned out to be a great challenge. Theoretically, it could be a robust free label sensor and it was proposed as a practical and dynamic tool able to carry out a fast and reliable detection of biomolecules.

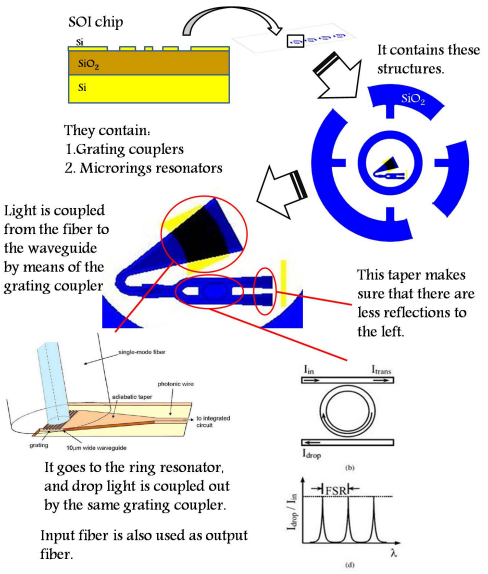

Figure 7.1: Structure: Microrings resonators and grating couplers

It consists of the adaptation of a microring resonator on the tip of an optical fiber. For that, grating couplers are needed to couple light from the fiber to the ring and viceversa. This structure is illustrated in figure 7.1.

In chapter 2, Simulations, the structure of this fiber probe sensor was simulated and compared with other two sensors. One of them was a Silicon-on-Insulator chip sensor, that consists of a microring resonator on a SOI chip, and the second one was a second fiber probe sensor, where the waveguides where on top of the SU-8, rather than embedded in it. Figure 7.2 illustrates them.

Results of this chapter confirmed that SOI chip sensor is very sensitive. However, it is not a practical and dynamic tool because it is needed a complicated setup to realize measurements.

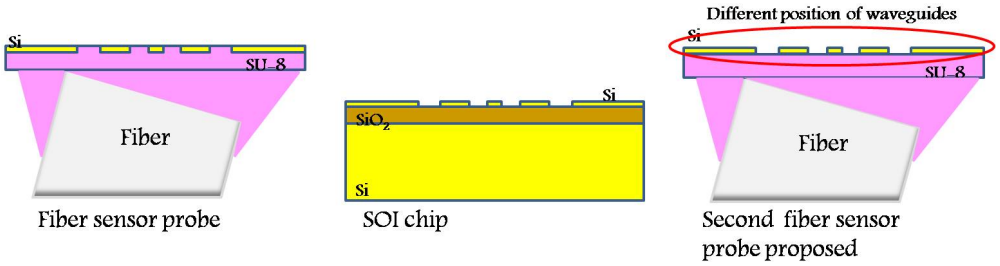

Figure 7.2: Compared designs.

The sensitivity of the second fiber probe proposed is the highest of the three structures for TE mode. The strategic position of the waveguides and the small confinement of the mode, due to the small contrast of the refractive index in the structure are two reasons that make them more sensitive than SOI chip. The walls of the waveguides where the electrical field is stronger, are exposed to the changing environment, whereas in our sensor probe design, these walls are surrounded by SU-8. It explains why its sensitivity is also higher than of our sensor probe. This advantage regarding our fiber probe proposed, entails a complicated and expensive fabrication process. This is the reason why this second fiber probe proposed was ruled out.

The first fiber probe sensor is the handiest and cheapest sensor. In addition, this fiber probe could be connected to any measurement equipment in a fast and comfortable way, and carry out a fast and reliable detection of biomolecules. The detection without the need of any fluidic or a complicated setup to perform the measurement and the use of this tool for in-vivo detections are also advantages of this fiber probe sensor. These are the reasons why we focused our research on them.

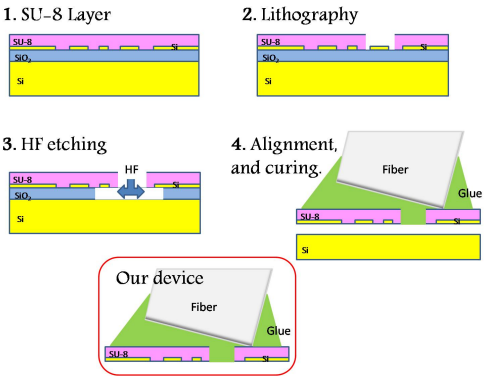

Figure 7.3: General sketch process 1.

Three different processes have been tried in order to fabricate it and to obtain good results as biosensor, nonetheless none of them were successful as of yet.

Process 1: Etching before sticking took most of the time of the work performed. It consists of four steps illustrated in figure 7.3.

The development was performed optimizing each step of the process, even another step was added, this is the HF dip before the SU-8 layer deposition, to

remove the possible native SiO_2 created on the Si waveguides surface and to optimize the adhesion of our structure to the fiber.

Measurements of the transmission after each step of the process were carried out. The signal showed resonances shifted after each step due to the change of the effective index on the sensor surface. After HF underetching, no more resonances were found. A deep investigation to find out the reason of the problem was carried out.

First idea was the replacement of the HF used, after observing that this HF could go through the SU-8 layer, underetching the sample without any lithography step. Buffered HF was proposed as solution, but it needed a long time to underetch the sample and SU-8 didn't resist

Finally some pictures taken by the SEM demonstrated that the structure was collapsed after the underetching.

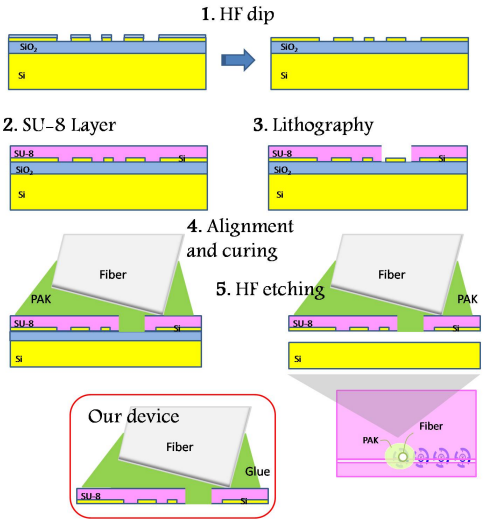

Figure 7.4: General sketch process 2.

The second process, Process 2: Etching after sticking, was very similar to the first one. It was developed in order to avoid the collapse problem of process 1. It consists of the same five steps of the process 1, but changing the order of the two last steps. An overview of the process is illustrated in figure 7.4.

Observing this sketch, the alignment and curing before the underetching require moving the chip and the fiber between both steps. For that reason the drop of PAK, glue used to stick fiber and chip, should be big enough to allow that the fiber held the chip. This was a problem, as the big drop of PAK prevented that HF began the underetching near our structure, consequently, this step took too long time, and the adhesion between sample and fiber was damaged. SU-8 was proposed to replace PAK, but results didn't improve.

Process 3: Removing of Si substrate and SiO_2 was performed as last alternative to obtain some good results. The main idea was to remove each layer of

the chip from the bottom, in order to leave just the Si waveguides stuck to the fiber. This process consists of six steps that are illustrated in figure 7.5.

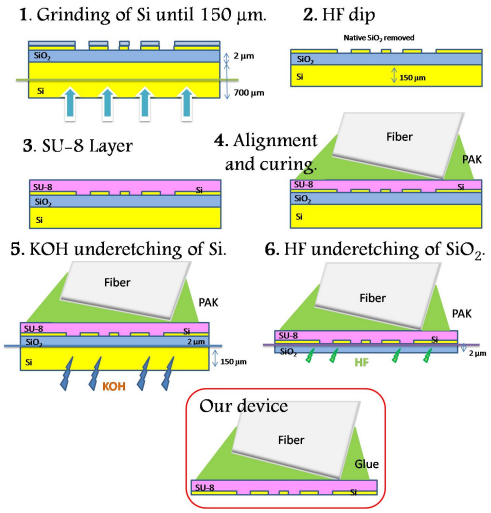

Figure 7.5: General sketch process 3.

Some difficulties were found developing this process. The most important was the fall of the sample after some time in KOH. The immersion in KOH should be approximately 150 min to remove the 150 μm of Si substrate left after the grinding. PAK, used as glue, came unstuck after one hour into KOH.

After trying some ideas, the need of protection of the sample and the fiber from KOH was the only possible solution. For this, wax was used to cover the sample and the fiber. The next problem found was the melting of the wax at 75^{o}C, temperature of KOH solution required to underetch Si. The wax melted went underneath the sample making impossible the underetching. After 150 min of immersion, the sample wasn't underetched at all.

Despite the lack of success at this stage, many processes were developed, and three promising future lines of research have been identified:

1. The research on the optimization of the SU-8 layer thickness that avoids the collapse of our structure.

2. Possible redesign of the mask used during the lithography. A possible option is illustrated in figure 7.6. The first aperture done near the rings could control the size of the drop, allowing the HF underetching by means of the second aperture. A redesign of the chip would be also necessary, to add SiO_2 where the apertures would be done.

Figure 7.6: Possible sketch for a future mask

3. The research on a product that resists KOH, and protects SU-8, sample and fiber would solve our problem, providing as result our device.

The work performed in this thesis provides an excellent basis from which to start this research.

List of Figures

Bibliography

[1] R. Ince and R. Narayanaswamy, "Analysis of the performance of interferometry, surface plasmon resonance and luminescence as biosensors and chemosensors.," *Analytica Chimica Acta*, no. 569, 2006.

[2] M. Z. A. Peter Schuck, *Protein interactions: biophysical approaches for the study of complex reversible systems*. ISBN 0387359656, 9780387359656, Springer, 2007.

[3] F. Vollmer, D. Braun, and A. Libchaber., "Protein detection by optical shift of a resonant microcavity.," *Applied Physics Letters*, vol. 80(21):40574060, 2002.

[4] C.-Y. Chao, W.Fung, and L. Guo, "Polymer microring resonators for biochemical sensing applications.," *IEEE*, vol. Selected Topics in Quantum Electronics, no. 12(1):134142, 2006.

[5] I. Christiaens, *Verticaal gekoppelde microringresonatorengefabriceerd met waferbonding*. PhD thesis, INTEC, 2008.

[6] M. Vanhoutte, "Biosensors based on circular resonators with vertical outcoupling structures," Master's thesis, Department of Information Technology , Faculty of Engineering, Ghent University, 2007.

[7] K. De Vos, I. Bartolozzi, E. Schacht, P. Bienstman, and R. Baets., "Silicon-on-insulator microring resonator for sensitive and label-free biosensing.," *Optics Express*.

[8] F. V. Laere, G. Roelkens, M. Ayre, J. Schrauwen, D. Taillaert, D. V. Thourhout, T. F. Krauss, and R. Baets, "Compact and highly efficient grating couplers between optical fiber and nanophotonic waveguides," *Light Technology*, vol. 25, no. 1, 2007.

[9] P. Dumon and D. Taillaert., "Building a vertical fibre coupling setup. silicon photonics platform,," *Silicon Photonics Platform*, December 2006.

[10] T. Claes, "Theoretical resonance wavelength shift due to effective index change taking dispersion into account," 2008.

[11] MicroChem, "Nano SU-8 negative tone photoresist formulations 2-25," *www.microchem.com*.